Chapter 5

Tip Simulation Results

After an extensive discussion concerning the current literature available on turbine blade tip research in Chapter 2, an overview of the tip geometry and test matrix in Chapter 3 and finally a description of the computational methodology in Chapter 4 the results of the study are presented in Chapter 5. Predictions of thermal and flow characteristics within the tip gap and surrounding area will be presented in four sections within this chapter. In Section 5.1, termed geometry 1, results are shown for cases with a baseline flat tip and no coolant injection at a small and large tip gap. Section 5.2, termed geometry 2, adds a twist to the baseline flat tip by adding a dirt purge cavity and no coolant injection, again with a small and large tip gap. This geometry allows for the investigation of flow field effects when a purge cavity is located in the blade tip. In Section 5.3, termed geometry 3, results are shown for cases where coolant is injected through two dirt purge holes. Cooling levels of 0.05%, 0.10%, 0.19%, 0.29% and 0.38% of the core inlet flow are studied for both a small and large tip gap to explore thermal and flow effects within the passage. Finally in Section 5.4, termed geometry 4, dirt purge and microcircuit coolant are injected into the passage. Total cooling levels of 0.5%, 1.0%, 1.5% and 2.0% of the core flow are utilized in an effort to effectively cool the tip.

Some of the thermal and flow phenomena considered include the formations of a pressure side and suction side vortex, the blockage of tip leakage flow due to blowing from the dirt purge and microcircuit, flow and thermal fields within the turbine passage, adiabatic effectiveness, pressure contours and distributions, and in-plane flows through the dirt purge and microcircuit ducts.

5.1 Geometry 1 – Flat Tip with No Blowing

The first geometry of the tip study consisted of a flat tip with no coolant flow and a small and large tip gap. These two cases served as a baseline, providing a basic

understanding of various flow features before the introduction of coolant or other geometric features. Figure 5.1 shows pressure contours along the blade tip and shroud for a small and large tip gap with the pressure non-dimensionalized by the inlet pressure conditions and given in C_p units. A close investigation of this figure shows some variation between the two tip gaps. Pressure along the shroud is very similar between the two tip gaps, especially around the leading edge, but there are some noticeable differences around the mid-chord. In particular, notice the larger low pressure region, $C_p = -10$, along the pressure side of the blade for the large gap when compared to the small gap. This larger low pressure zone indicates that there could be a higher velocity and possibly additional tip leakage than what was seen with the small gap or it could be due in part to greater flow separation. Also noteworthy with the shroud pressure contours are the variations along the suction side of the blade within the main passage. The lower pressures of $C_p = -8$ to $C_p = -10$ around the mid-chord indicate higher velocity flow and tend to highlight the location and formation of the tip leakage vortex, which will be discussed later in some detail. The large tip gap has both a lower and larger area of low pressure when compared to the small tip gap case, indicating the vortex increases with tip gap height. Along the pressure side of each blade, within the main passage, the pressure distribution between the two tip gap cases remains constant.

Pressure contours along the tip surface in Figure 5.1 continues to illustrate the same trends seen with the shroud contours. The low pressures regions ($C_p = -12$ to $C_p = -14$) along the pressure side of mid-chord indicate the possibility of a flow separation zone. With the pressures lower on the large tip gap case it appears as though any flow separation is more substantial with a large tip gap. There is little variation between pressure contours outside of the mid-chord region at either the leading edge or trailing edge, a trend seen throughout the shroud as well. At the leading edge there does appear to be a slightly larger high pressure zone ($C_p = -2$) with the large tip gap. A quick comparison of pressure variations between the tip and shroud shows similar contour placement and magnitude in the leading edge. Moving to the mid-chord and trailing edge, pressures are slightly lower along the tip when compared to the shroud.

Figure 5.2a-b shows the contours static pressure distribution and velocity vectors in a plane cut near the mid-chord. The approximate location of the data plane is depicted

by the dark lines through each blade tip along the right-hand side of the figure. Notice in both Figure 5.2a-b, the velocity vectors indicate flow being drawn into the tip gap along the pressure side of the blade and the subsequent low pressure zone as flow enters the gap region. This low pressure may be attributed to two things including: the increase in velocity as flow enters the tip gap and the flow separation from the blade tip. Particularly evident at the large tip gap, is the separation zone that is shown with low pressure contours (C_p= -14) and vectors indicating flow separating around the area just inside the tip gap. In Figure 5.2a, vectors show flow directed toward the tip gap with the size of the vectors increasing as the distance from the gap is reduced, a result of accelerating flow. The vectors reach their largest size within the gap. This same phenomena is also depicted in Figure 5.2b with a significantly greater region affected by the tip gap. The magnitude of the vectors outside of the gap is considerably greater with the larger tip gap and the low pressure zone has propagated further into the mainstream. The size of the velocity vectors within the tip gap does not seem to vary much when comparing the large and small tip gaps meaning there may only be added mass flowrate with the increase in gap size.

Figure 5.3a-b shows contours of non-dimensional velocity through the center of the small and large tip gaps where velocity magnitude has been divided by the inlet velocity. Comparison of the contours at the small and large tip gap shows little variation in velocity around the leading edge with higher velocity around the mid-chord for a large tip gap. The small tip gap experiences velocities that are about 2.5 times that of the inlet velocity, while the large tip gap velocities that approach 3 times that of the inlet velocity.

Another interesting comparison within the tip gap involves the examination of the overall mass flow through the tip gap. Table 5.1 contains a large amount of data pertaining to tip gap leakage for various cases and calculations methods that were explored, but paying particular attention to two cases: (1) a small tip gap with a flat tip and (2) a large tip gap with a flat tip, each with no coolant, the tip leakage flow as measured computationally is denoted in the column labeled *CFD,* in which the leakage flow is given as a percentage of total core flow. The small tip gap has a leakage of 1.3% as measured by the CFD while the large tip gap has leakage of 3.8%. Recalling that the large tip gap is three times the size of the small, we see that the average flow velocity

through the tip remains constant as three times the small tip gap flow of 1.3% is 3.9%, very close to the 3.8% obtained for a large tip gap. It appears as though the velocity profiles at the middle of the tip gap vary between the two respective tip heights as seen with Figure 5.3a-b, but the average velocity is steady.

The tip leakage mass flow rates in the *CFD* column as discussed in Table 5.1 were obtained by establishing several computational planes within the tip and recording the mass flowrate. These planes are shown in Figure 5.4e and were placed by first investigating the streamlines through the tip gap in Figure 5.4a-d to ensure all of the flow across the tip was included within the two planes. The leakage flow through the tip gap was then calculated by calculating the mass flowrate through the two respective tip planes. The leakage mass flowrate was then divided by the inlet mass flow to obtain the data shown in the *CFD* column. Another novel attempt to predict tip leakage was attempted. This method involved calculating the average pressure drop between the pressure and suction sides of the blade using both the tip and shroud pressures to back out a tip flow. Having the average pressure values along the pressure and suction side of the blade, a simple Bernoulli relation was applied with the two averaged pressures producing an average velocity through the tip based on the pressure drop. From this velocity, a mass flow rate could be derived. The predicted flows using tip and shroud pressures are shown in Table 5.1 under *Tip ΔP* and *BOAS ΔP* and compared to the actual CFD mass flowrate (*CFD*). The variations in the tip and BOAS predicted mass flow from the CFD are also presented in the two columns on the far right. It appears as though shroud (BOAS) pressures accurately predict mass flow, typically varying by less than 5% from the mass flowrate, while tip pressures do not provide the precision of the shroud. All of these measurements were made with computational data and may help to predict experimental tip leakage as it is possible to measure pressures along the shroud from which a mass flow could be derived.

Streamlines released upstream of the blade indicate the flow patterns through the tip gap region as shown Figure 5.4a-b for a small and large gap, respectively. The streamlines are released from a plane that is 1.5 tip gap heights below the shroud meaning the lines are at the same relative location within the gap for both the small and large tip gap. For a small tip gap, measuring 3mm at a 12x scale, the streamlines were released

4.5mm below the shroud while for the large tip gap streamlines were seeded from 13.5mm below the shroud for a 9mm tip gap of the same scale. The lines are colored by a non-dimensional spanwise velocity that results in a green/yellow color (w=0) for streamlines traveling in a horizontal path with blues and reds occurring for large negative and positive spanwise velocity components.

Looking at Figure 5.4a-b one can notice the formation and development of the tip leakage vortex along the suction side of the blade. As shown by the pressure contours of Figure 5.1a-b, the leakage vortex is significantly bigger for the large tip gap. A comparison of the streamlines from the small and large tip cases shows additional flow traveling through the large tip gap. This is evident by examining the lack of streamlines near the pressure side of the trailing edge in Figure 5.2b versus Figure 5.2a. It is also apparent near the leading edge of the blade that there is a longer streamline distance across the tip for the larger tip gap when compared to the small tip gap. The streamlines from the larger tip gap exit onto the suction side further downstream resulting in a greater velocity differential between the passage and tip leakage flow. It is this velocity differential combined with a larger leakage flow at the large gap that leads to a larger vortex formation than the small tip gap.

Figure 5.5a-b shows the tip leakage vortex for the both the large and small gap at the SS6 plane as defined in Chapter 4. These secondary flow vectors are shown for a plane that is located along the latter portion of the suction side near the exit of the blade passage (94% axial chord). The plane is taken normal to the suction side surface and is depicted with a black line along the suction side of the blade in Figure 5.4a. The transformed v- and w- components (Vn and Vz) are plotted as a function of the distance perpendicular to the blade (y/P) and the distance down the shroud (-z/S). A more detailed discussion of the method is presented in Chapter 4. These two images show the size of the tip leakage vortex for the two tip sizes with the approximate location of the tip gap noted on each plot. For the large tip gap of Figure 5.5b, the vortex dominates nearly the entire plot and is centered at y/P = 0.20 and z/S = -0.07. A clockwise rotation can be seen throughout the entire figure and is both aerodynamically and thermally undesirable as this vortex causes pressure losses and high turbulence. Predictions indicate that the vortex is shifted slightly closer to the blade surface for the small tip gap which is centered

at y/P = 0.10 and z/S = -0.05. Unlike the large tip vortex, the vortex that occurs for a small tip is substantially smaller with a spanwise region from z/S = 0 to z/S = -0.15 affected. The outward flow seen in Figure 5.5a near y/P = 0.3 is a result of the fluid being entrained into the wake region of the adjacent blade. Additional secondary flow vectors from all of the suction side (SS) and pressure side planes (PS) as defined in Chapter 4 can be seen in Appendix C for these two baseline cases as well as for other selected cases.

In Figure 5.6a-b a pressure side plane (PS2) is shown with the small and large tip gap, respectively. The plane is located just below the dirt purge cavity along the pressure side of the blade at 30% of the axial chord and is displayed in Figure 5.4a with the black line along the pressure side of the blade. For these two cases we see flow entering the tip gap region at y/P = 0 and z/S = 0 with the approximate height of the tip gap noted by the dashed lines. Similar trends were seen in Figure 5.2a-b, which cut through the mid-chord region of the blade along the pressure side. The large tip gap flow in Figure 5.6b is drawn in from beyond the plot borders of y/P = 0.35 and z/S = -0.30 while the small tip gap of Figure 5.6a only effects a region from y/P = 0.20 and z/S = -0.20. This is a substantial variation based on geometry.

Another interesting feature to study is the dirt purge or lack thereof. Cross-sectional views through the leading edge are shown in Figure 5.7a-b and highlight the location where the dirt purge will be placed in subsequent tests. These two images will serve as baseline scenarios for what one could expect without this cavity. Each image has velocity vectors showing the trajectory of the flow at specific locations with non-dimansionalized in-plane velocity contours overlaid. In these figures value of z/S = 0 corresponds to the shroud, but it should be noted that the distance along the horizontal axis is arbitrary. An examination of Figure 5.7a shows a small tip with the velocity slowly increasing as the flow moves from left to right, varying from about 1.5 times the inlet velocity to values of 2 times the inlet velocity. In Figure 5.7b, which shows a large tip, the velocity again increases moving from left to right with some variations from the small tip case. Higher velocities are seen with the large tip gap and occur earlier when compared to a small tip gap. Ultimately, a velocity twice that of the inlet velocity seen at a position of x/P = 0.15 at the large gap while that same velocity is not obtained until x/P

= 0.20 at the small gap. The velocity vectors show the flow to be directed across the tip with little vertical movement.

5.2 Geometry 2 – Dirt Purge Cavity with No Blowing

A variation on the first geometry led to the creation of a tip containing a dirt purge cavity with no blowing. This geometry was studied to examine the effects of the dirt purge geometry on the tip gap flow characteristics. In the event that the dirt purge becomes clogged with debris a situation would arise in which there would be a non-blowing dirt purge cavity for which this geometry applies. Figure 5.8 shows pressure contours along the blade tip and shroud for the two tip gaps. Using the flat tip cases of Figure 5.1 for comparison one can see there are only a few subtle variations with the addition of a dirt purge cavity placed within the tip when compared to a flat tip. These pressure changes between geometry 1 and geometry 2 are primarily found around the leading edge, but any variations downstream will also be explored.

Looking first at the shroud in Figure 5.8, the only differences between the flat tip and tip with a dirt purge cavity appear to occur around the cavity in the leading edge area. This alerts us to the fact that the dirt purge may only provide localized flow and thermal effects. A high pressure zone is present at the location of the purge cavity for both a small and large tip. This high pressure relates to a low velocity region. Ultimately, the velocity of flow in the dirt purge slows because of flow stagnation in the cavity as well as an expanding area for the flow to travel as the fluid moves from the tip region into the combined tip and cavity region. The size of the high pressure area is slightly bigger for the large tip, as there is more leakage flow and a higher velocity, thus there is more dynamic pressure to dissipate during the area expansion. From the mid-chord to trailing edge there is little change from the baseline geometry on both small and large tip gap.

Moving from the shroud to the tip contours of Figure 5.8 one can see high pressure near the back of the dirt purge cavity and low pressure just downstream of the cavity on both tip gaps. The high pressure region shows a stagnation zone at the bottom of the cavity as flow impinges on the dirt purge wall, while the lower pressure just

downstream of the cavity shows the high velocity of the flow as it exits the cavity and tries to re-enter the main leakage flow path. A comparison of both large and small tip gap cases to the flat tip cases as depicted in Figure 5.1 shows some slight pressure variations in the mid-chord region. At the small gap the pressures are lower than seen on the flat tip case, which relates to a higher tip velocity. The large tip gap may experience a slight increase in pressure from the baseline. The small changes in mid-chord pressure could be leakage flows around the leading edge being modified due to the purge cavity.

Figure 5.4c-d show streamlines released just upstream of the blade at 1.5 tip gaps below the shroud for both tip gaps, similar to the data presented in Figure 5.4a-b for a flat tip. Investigation of the suction side tip leakage vortex shows little if any variation in the size of this vortex with the addition of a dirt purge cavity. The only noticeable differences occur around the leading edge. Looking at the purge cavity for both a small and large tip, one can see streamlines converging into this cavity. The streamlines appear to show an increased tendency to be pulled into this cavity for a small tip. One might also argue there is a slight change in leakage flow just below the dirt purge holes, which could explain the change in mid-chord pressures seen in Figure 5.8. As the streamlines reach the back of the cavity the velocity slows before a large jump in spanwise velocity. This high spanwise velocity is indicated by the red coloring of the streamlines that generally maintain a level trajectory until swept into the leakage vortex. Overall, the tip leakage does not seem to vary substantially with the addition of a purge cavity at either tip gap height. This conclusion stems from looking at the streamlines on the pressure side of the blade, near the trailing edge. These streamlines remain very similar to those of the flat tip cases and show that the same number of streamlines enter the tip gap whether it is flat or has a cavity.

Figure 5.5c-d shows little variation in the size and location of the tip leakage vortex when compared to the flat tip geometry as seen in Figure 5.5a-b. The same plane (SS6) was used to highlight the location of the tip leakage vortex for geometry 1 and geometry 2 and any alterations between cases have gone unnoticed by the author. A comprehensive investigation leads to the conclusion that there are no changes in the positioning and magnitude of the tip leakage vortex when a dirt purge cavity is added over the leading edge region.

Examining a plane on the pressure side of the blade (PS2) in Figure 5.6c-d there is once again no change in the tip leakage flow with the addition of a purge cavity in the tip. This plane, more-so than the suction side plane (SS6), would have been expected to show possible changes in the flow patterns from the flat tip cases, as it is located just below the dirt purge on the pressure side of the blade. We see the large tip gap case of Figure 5.6d has flow entrained from a region stretching beyond y/P = 0.35 and z/S = -0.30 while the small tip gap case of Figure 5.6c affects a region spanning from y/P = 0.20 and z/S = -0.20. This remains unchanged from the flat tip cases.

A cross section through the leading edge and dirt purge cavity provides some interesting insights into the tip leakage flow patterns. Figure 5.7c-d depicts the predicted velocity vectors and contours within the purge cavity for a small and large tip, respectively. The in-plane velocity contours have been non-dimensionalized by the inlet velocity. Velocity contours of the large tip gap show higher velocities than what is seen in the small tip gap. The size of the low velocity region, located at the point at which the tip gap expands with the dirt purge cavity (x/P = 0.03), remains constant between the small and large tip gap with the region extending out to a distance of x/P = 0.10 along the horizontal axis. Images at both tip gaps show flow vectors being diverted into the cavity and their subsequent return to the main into the main tip leakage flow. The return of the flow into the tip results in high velocities just downstream of the purge cavity that are particularly evident closer to the shroud. For the small and large tip velocities tip velocities reach levels greater than 2 times the inlet velocity. Comparison of these results to the flat tip show dramatic variations as the area expansion greatly effects the flow around the leading edge.

5.3 Geometry 3 - Dirt Purge with Blowing

Dirt purge holes are present in most turbine blades in use today. They are a necessary part of blade construction and serve to exhaust dirt and debris from the turbine blades in order to prevent the clogging of important film cooling holes. A study of dirt purge cooling was examined as a baseline cooling case with an entire flow and thermal

analysis performed with comparisons made to the first two geometries when appropriate. Comparisons of dirt purge cooling to combined microcircuit and dirt purge cooling will also be made in the following section. Presented in this section is a comprehensive investigation of the flow and thermal characteristics for geometry 3, a dirt purge cavity with cooling flow.

The original plan of study for the tip geometry called for the examination of microcircuit and dirt purge cooling with blowing levels of 1.0% and 1.5% core flow. The investigation of these two blowing levels combined with two tip heights began the research. Initial work involved studying the coolant flow to each duct of the microcircuit and dirt purge hole to obtain a flow distribution plot. The flow through each of the sixteen microcircuit and two dirt purge holes was documented for each of the four cases. Results showed that the relative percentage of coolant flow going to each hole remained constant at each of these four cases (an expected result because the flow is pressure driven and the pressure around the blade remains constant for each test). Calculations showed that each dirt purge hole released approximately 10% of the overall coolant flow for a total of 20% of the coolant air coming from the dirt purge ducts. Thus, using the original microcircuit cooling requirements of 1.0% and 1.5% two new values of 0.19% and 0.29% were computed for only dirt purge flow. This resulted in the same amount of coolant exiting the dirt purge holes for a case with 0.19% dirt purge cooling as would be exiting the dirt purge holes for a combined dirt purge and microcircuit test with 1.0% coolant. In addition, a case with dirt purge cooling of 0.29% corresponds to a combined dirt purge and microcircuit case of 1.5% coolant. Additional dirt purge cooling cases with coolant levels of 0.05%, 0.10% and 0.38% core flow were also examined to obtain a comprehensive analysis of the cooling trends seen from dirt purge cooling.

Figure 5.9 shows pressure contours along the shroud and tip for a small tip gap with dirt purge blowing. Coolant mass flowrate levels of 0.05%, 0.10%, 0.19%, 0.29% and 0.38% core flow were examined and will be presented throughout the dirt purge study. Looking first at the shroud, it is evident that pressure contours downstream of the dirt purge remain constant with all blowing levels. This trend was also seen when pressure was examined with a dirt purge cavity and no blowing. Looking back to the leading edge we see that as coolant levels increase from low to high, white regions

develop on the shroud. These white areas are the result of non-dimensional pressures exceeding the limits of the specified contour levels. The high pressure seen in these areas can be attributed to the high velocity dirt purge jets impinging on the shroud and creating a stagnation region in which the pressure exceeds the scale. Also worth noting is the low pressure zones, where $C_p = -10$, located around the cavity that are increasingly present with additional blowing. These low pressures indicate high velocities, and these higher velocities result from the additional coolant added to this region. Pressure contours along both the suction and pressure sides of the blade that are within the main passage remain constant as the blowing level increases from 0.05% to 0.38%. Around the stagnation location the pressure increases with additional coolant, transitioning from areas of $C_p = -3$ to $C_p = 0$. This is the result of a more effective flow blockage from the dirt purge coolant that results in additional flow stagnation and thus higher pressures.

Looking at the tip pressure contours of Figure 5.9 one can see that there are many variations in these five images. As expected the leading edge shows a continual evolution with the addition of coolant. The pressures near the blade stagnation increase as coolant is added, which was also observed along the shroud. In addition, there is trend showing lower pressures within the dirt purge cavity as more coolant is added. This low pressure ultimately means higher velocities within the cavity, which is expected with more dirt purge coolant. The significant changes in pressure throughout the mid-chord region were somewhat unexpected. Examination of the shroud contours shows little change in pressure as coolant levels vary, but the pressure around the tip at the mid-chord shows a constant, but steady reduction indicating a possible increase in the tip leakage flow for increased dirt purge blowing. One must consider that with additional coolant being added to the flow there is also an added flow blockage over the leading edge. Instead of tip leakage flow traveling over the leading edge, it is simply diverted further back onto the blade and towards the mid-chord. The constant pressure decrease along the mid-chord coincides with added upstream blockage.

A closer examination of the tip gap leakage flow is made in Table 5.1. This table shows that there is no significant change in tip leakage mass flowrate when the dirt purge blowing is changed from 0.19% to 0.29% nor is there any variation in leakage when comparing to the flat tip gap cases. We can see this by looking at the *CFD* column in

which the dirt purge cases (at both tip gaps) experience nearly the same leakage seen for the flat tips. Thus far, it appears that tip gap height is the only factor controlling the amount tip gap leakage flow. Figure 5.3c-d depicts non-dimensional velocity contours in a plane cut through the middle of a small and large tip gap, respectively, with 0.29% blowing. The contours show low velocity at the leading edge of both blades due to the dirt purge cooling inhibiting the flow with the small tip gap having the lowest velocities. Along the mid-chord the large tip gap exhibits higher velocities than the small gap, but once again Table 5.1 shows the average velocity through each gap remains unchanged with tip gap height. The large tip gap continues to experience a tip leakage amount that is three times larger than the small tip gap, when the height variation between the two tip gaps is also three.

Pressure contours with a large tip gap and dirt purge cooling are presented in Figure 5.10. Notice along the shroud, as was seen with a small tip gap, that there is no variation in the mid-chord, and trailing edge region between any of the five blowing ratios. Around the dirt purge there are significant local pressure effects due to dirt purge blowing. Once again, there is high pressure where the dirt purge ducts impact the shroud and the pressure levels around the dirt purge stagnation points increase with added cooling. For 0.05% and 0.10% blowing, the dirt purge jets do not impact the shroud. This differs from the small tip gap cases in which only 0.05% blowing did not impact the shroud. At the large tip gap, the momentum of the tip leakage seems to dilute the cooling. As the injection levels increase one can also see the higher pressures at the blade stagnation.

Investigation of the tip pressure contours in Figure 5.10 shows two distinct contour maps at the leading edge. The pressures along the tip seen at cooling flows of 0.05% and 0.10% seem to be very similar while conditions at 0.19%, 0.29% and 0.38% also exhibit the same characteristics. This is the result of two different flow patterns that may have developed. In the mid-chord area there is a slight variation along the suction side between the high and low cooling flows as defined above, but along the pressure side there is a low pressure zone ($C_p = -14$) that remains constant. This low pressure zone is indicative of a possible flow separation that has been discussed throughout this chapter. The lack of pressure variation along the mid-chord with a large tip gap could result

because the of the dirt purge coolant being ineffective at blocking the flow. Ultimately, the following figures in this section will show that a small tip gap with higher blowing rates provides substantial flow blockage over the leading edge, while the large tip gap does not experience the same blockage at any of the tested blowing rates.

Figure 5.11a-b depicts streamlines released upstream of the blade at 1.5 tip gaps below the shroud for a blowing level 0.29% and a small and large tip, respectively. In Figure 5.11a one can clearly see the streamlines being diverted from the leading edge region by the dirt purge flow. This figure though should not be interpreted to mean that there is no tip leakage around the purge cavity because there is still some hot gas penetration into the region. We are only looking at streamlines released from a single plane upstream that allow us to obtain a general understanding of the flow. Looking at the large tip gap as shown in Figure 5.11b there is minimal effect on the mainstream flow patterns. Along the suction-side, just above the leading edge of the blade for the small tip gap notice the large number of streamlines that are not passing over the blade when compared to the large tip gap. Along the trailing edge pressure-side of the blade there is also a substantial number of streamlines that do not pass over the small tip when compared to the large tip, a trend that is also seen for non-blowing cases as well.

Some interesting comparisons can be made between the two cases with dirt purge blowing (Figure 5.11) and the four cases without blowing (Figure 5.4). The tip leakage vortex does not seem to change substantially with the dirt purge blowing, but along the suction side of the blade just above the purge cavity there is a noticeable change in the number of streamlines that are diverted into this area with the addition of blowing for a small tip gap.

Figure 5.12a-b shows a suction side plane (SS6) plotting the secondary flows of the tip leakage vortex. Comparison of the two vortices in Figure 5.12a-b to those vortices that appear with no blowing as shown in Figure 5.5a-d do not initially yield many differences. However, a closer look does provide some subtle differences that should not go unnoticed. For the small tip gap vortex of Figure 5.12a there is some variation in the vector size and direction near $z/S = -0.15$ and $y/P = 0.2$-0.35. The vectors of Figure 5.12a are somewhat smaller and have a more horizontal direction than those of the baseline case with a flat tip in Figure 5.5a. Overall, the center of the vortex and the main flow

features are unchanged by the purge blowing. Comparing Figure 5.12b to the flat tip of Figure 5.5b yields similar results to those seen for the small tip gap. The vector magnitude is smaller at and below z/S = -0.25. The smaller vectors may be a sign of a slightly smaller vortex when there is dirt purge blowing, but the overall flow dynamics remain the same with the addition of dirt purge coolant.

Streamlines released from inside the plenum and colored by non-dimensional temperature are shown in Figure 5.13a-d for blowing levels of 0.19% and 0.29% at both tip gap heights. The high blowing ratio of 0.29% is presented in Figures 5.13a-b with the small tip followed by the large tip. Notice that with the small tip, there is an increase in coolant distribution when compared to the larger tip gap. This increased spreading can be explained by a number of factors. Most significant is the effect of the increase in mass flow with a large tip gap. At a large tip gap this leakage serves to dilute the coolant more than would be seen with a smaller gap. This dilution results from high velocity tip leakage flow that has substantial momentum and does not permit dirt purge cooling to penetrate the large gap region as it would the small. The small tip gap has very good coverage over the leading edge. In fact, there is a slight blow-off into the main passage before the cooling flow is pushed into the tip gap near the mid-chord. Reducing the coolant levels to 0.19% as shown in Figure 5.13c-d shows a reduction in the size of the cooling area for both large and small tip cases. This comes as no surprise as a decrease in coolant implies lower velocities and less momentum to block leakage flow. An astute observer may notice that with a small tip gap the dirt purge flow is shown to cover most of the leading edge and this was confirmed with the streamlines released upstream of the blade in Figure 5.11a that are diverted around the leading edge. However, the large tip gap streamlines released in Figure 5.13b and Figure 5.13d lead the reader to believe the leading edge region covered by streamlines is cooled, but this is not true. Looking at Figure 5.11b, which depicts a large tip and 0.29% coolant flow, we see that streamlines released upstream of the blade penetrate into the leading edge allowing hot gases into the region.

Figure 5.14a-b shows a pressure side plane (PS2) for a case of 0.29% dirt purge cooling with a small and large tip, respectively. These planes are taken at a similar location to those seen in Figure 5.6a-d for cases without blowing, and there are not too

many noticeable differences. Only in Figure 5.14a is there any variation between blowing and non-blowing cases. Along the shroud at z/S = 0 and y/P = 0.075 there is evidence of flow being deflected by small amounts of dirt purge blow-off into the pressure side of the main passage. Overall, the dirt purge flow seems to have minimal effects on the tip leakage flow in this area.

Adiabatic effectiveness contours are shown in Figures 5.15 and 5.16 with dirt purge cooling. Figure 5.15 shows five blowing ratios at a small tip gap while Figure 5.16 shows the same blowing ratios at a large tip gap. Starting with the shroud contours in Figure 5.15 one can see an increase in cooling effectiveness as more coolant is added. At low percentages of cooling flow (0.05% and 0.10%) the velocity and momentum of the coolant is low, which inhibits its ability to reach the shroud, not to mention there is just not enough cooling mass. With the addition of more coolant flow there is additional cooling capacity as well as an increase in the momentum of the cooling jets to infiltrate deeper into the tip leakage flow and impact the shroud. With coolant levels of 0.29% and 0.38% there is sufficient coolant to the point where blow-off occurs onto the pressure side of the blade. At no point is the coolant predicted to reach the blade stagnation area.

Looking at the tip predictions of Figure 5.15 shows good tip cooling when coolant levels are at least 0.19%. As expected additional coolant provides better cooling coverage of the tip, improving from little cooling at 0.05% to almost full leading edge coverage at 0.38%. The effectiveness contours at the lower blowing ratios (0.05% and 0.10%) show the low momentum cooling jets being swept across the tip along with the hot tip leakage flow. Only as the cooling increases to the previously mentioned 0.19% is there enough cooling mass and momentum to penetrate upstream into the tip. When the blowing levels are at or above 0.19% a large region over the leading edge is cooled to levels approaching $\eta = 1$, indicating excellent cooling effectiveness. For all cases, the blade tip near the stagnation point is not cooled. The mid-chord and trailing edge are thermally unaffected by the dirt purge coolant. Looking at the pressure contours of Figure 5.9 shows good agreement with the thermal data presented in Figure 5.15. In particular, are the pressure contours along the tip that vary based on coolant flow. At low flow (0.05% and 0.10%) and high flows (0.19%, 0.29% and 0.38%) there are two basic

pressure contours that relate well to the two cooling patterns seen along the tip for the same flows.

Predicted cooling effectiveness drops off substantially when the tip gap is increased to its large height. Shown in Figure 5.16 are the contours for dirt purge blowing at a large tip gap. The shroud cooling improves from virtually no cooling at the lowest coolant level (0.05%) to very good coverage at the highest blowing level (0.38%), displaying the same steady improvement in cooling that was predicted for a small tip gap. The only $\eta = 1$ regions, indicating a highly cooled surface, are located where the dirt purge jets impinge on the shroud. This is in contrast to the small tip cases that had significant areas of very good adiabatic effectiveness surrounding the dirt purge holes. Tip gap leakage at this tip gap height is much greater allowing for significant mixing of the coolant and mainstream gases that results in a reduction of cooling. The pressure side blow-off is somewhat lessened in these cases when compared to the small tip gap. This blow-off is only noticeable at the highest blowing ratio (0.38%) compared to the three highest blowing ratios (0.19%, 0.29% and 0.38%) that experience pressure side blow-off with the small tip gap.

Tip effectiveness predictions for the large tip gap of Figure 5.16 due not follow the previous trends seen with the small tip and shrouds at both gap heights. Instead of more coolant increasing the tip cooling, the surface temperatures are predicted to actually maintain the same effectiveness levels or rise as coolant levels are increased from 0.05% to 0.38% cooling. Predictions indicate that some of the best cooling occurs for the lowest flow rates of 0.05% and 0.10%. This is due primarily to the low momentum coolant jets that remain attached to the surface of the blade and cool the tip just downstream of the purge holes. At the higher blowing rates computations suggest hot tip leakage slides between the tip and coolant air to block much of the high velocity coolant jet from mixing out and cooling the region. This phenomena was briefly discussed in Figures 5.11 and 5.13 when looking at the flow for a large tip gap. Streamlines released upstream of the blade were not shown to be greatly affected by the coolant in Figure 5.11, but the coolant streamlines that were released from the plenum appeared to cool the leading edge as shown in Figure 5.13. Only when cooling levels reach 0.38% does this decrease in effectiveness with the addition of coolant seem to end. Similar to the small tip gap cases,

there appear to be two different tip cooling patterns that occur at low flows (0.05% and 0.10%) and high flows (0.19%, 0.29% and 0.38%). These cooling patterns are reflected in the pressure contours of Figure 5.10 that can also be divided into two different contour patterns around the leading edge.

Figure 5.17a-d shows four cross-sectional views that have been cut through the center of the dirt purge cavity. Each cross-section has effectiveness contours and velocity vectors to show flow patterns. Looking first at Figures 5.17a and c, which are the small tip gap cases with cooling of 0.29% and 0.19%, respectively, we see excellent cooling along both the shroud and tip surfaces. In fact, the only $\eta < 1$ region in either plot is seen in Figure 5.17c at the leading edge of the purge cavity. Significant cooling for the small tip gap is achieved with both blowing ratios. At the large tip gap plots of Figure 5.17b and Figure 5.17d (0.29% and 0.19% cooling, respectively) one can see a variety of gradients throughout the region indicating a wide range of temperatures. Looking first to Figure 5.17b which shows cooling at 0.29% the coolant is shown leaving the two dirt purge holes, traveling through the cavity and tip gap before impinging upon the shroud. The impingement on the shroud causes the flow to spread across the surface before turning down toward to the tip creating small vortices. Unfortunately, the cool gases never fully reach the tip surface, as hot gases are seen saturating the area from upstream leakage and/or hot tip leakage slipping under the dirt purge coolant. In Figure 5.17d, which shows the coolant level reduced from 0.29% to 0.19% the same trends discussed at 0.29% are seen for this case with a slight reduction in cooling. Also noteworthy, is a comparison of these flows to those of the non-blowing cases as shown in Figure 5.7. In particular, the low velocity region at the leading edge of the dirt purge cavity that was present at the non-blowing cases (Figure 5.7a-d) has been reduced with dirt purge blowing, but one can still see hot gases, $\eta = 0$, around much of the cavity.

Pitchwise-averaging of adiabatic effectiveness provides an excellent method for comparing data from multiple cases as discussed in Chapter 4. Figures 5.18-21 present pitchwise-averaged data along the tip and shroud for the small and large tip gap. Finally, Figure 5.22 presents all of the data from Figures 5.18-21 in one plot in which an area-averaged effectiveness has been calculated for each of the dirt purge blowing tests and plotted against the coolant mass flowrate.

Figure 5.19 presents pitchwise-averaged effectiveness over the tip for a small tip gap with dirt purge blowing. The data in this plot provides valuable insights into the advantages or disadvantages of a cooling scheme. Notice that the two lowest blowing ratios (0.05% and 0.10%) provide very poor cooling when compared to the higher blowing rates that provide relatively good cooling over the leading edge. In fact, the only advantage seen between cooling levels of 0.29% and 0.38% is around the blade stagnation location of the leading edge ($x/B_x = 0$), everything else is nearly identical. A slight drop-off is seen with 0.19% coolant, but somewhere between 0.19% and 0.10% cooling there is a significant change in the flow physics, as discussed previously.

Pitchwise-averaged effectiveness for a large tip gap and dirt purge blowing is shown in Figure 5.19. These results show the best overall cooling to occur when the cooling flow is 0.05% with a general decline in effectiveness seen as additional coolant is added through the dirt purge. In fact, the worst results are seen with cooling levels of 0.19% and 0.29% before a slight improvement occurs at 0.38% cooling. In all cases the peak tip cooling is seen around $x/B_x = 0.1$, while $\eta = 0$ generally occurs around $x/B_x = 0.5$ to $x/B_x = 0.6$.

Results along the shroud are shown in Figures 5.20 and 5.21 for a small and large tip, respectively. The curves along both plots follow the same pattern with coolant flow seen to begin between $x/B_x = 0$-0.1 and ending near $x/B_x = 0.5$-0.7. The curves of Figure 5.20 show greater cooling effects with additional coolant than Figure 5.21. It appears that the curves of Figure 5.21 seems to be offset by approximately $\bar{\eta} = -0.1$ from its counterpart in Figure 5.20. It should be noted that while the contour plots of effectiveness in many cases show good cooling of the leading edge, the area of the shroud is considerable larger than that of the tip, so that these results will be inherently lower than those seen along the tip.

In Figure 5.22 all ten cases run with dirt purge cooling are presented. Area-averaged adiabatic effectiveness along the tip and shroud is plotted against the coolant mass flow rate for a total of four curves: (1) *small gap – tip*, (2) *small gap – shroud*, (3) *large gap – tip*, and (4) *large gap – shroud*. The averages along the shroud show continued cooling improvement as more coolant is added over the entire range of cooling. Small tip cases slightly outperform the comparable large tip cases. Each curve is of a

generally constant slope and shows no signs of decreasing. Effectiveness averages along the blade tip do not show the same trend seen along the shroud for the two different tip gaps. At cooling levels of 0.05% and 0.10% there is little change in the cooling for a small or large gap height, but as the cooling increases there are great variations. Predictions show superior results from the small tip cases in which area-averaged effectiveness increases to values near $\bar{\eta} = 0.40$ along the tip, while the large tip cases continue to remain very low over all of the cooling levels.

5.4 Geometry 4 – Microcircuit and Dirt Purge with Blowing

Microcircuit film cooling represents a relatively unexplored method in blade cooling. A detailed discussion of the geometry and other such pertinent information about the microcircuit was presented in Chapter 3. Composed of two regions, a leading edge circuit and a mid-chord/trailing edge circuit, there were a total of sixteen ducts providing coolant to the tip region. Figure 5.23 shows the location of each duct around the blade with a corresponding number. Microcircuit cooling offers the ability to provide very effective cooling through both internal convection/conduction and external film cooling. The intricate microcircuit ducts located throughout the tip allow for significant cooling to take place by internal convective heat transfer and conduction. As the cool microcircuit air leaves the microcircuit, it enters the main flow passage along the pressure side of the blade. Most of this coolant is pulled into the tip gap by the tip leakage flow thereby providing external film cooling over the tip. In some cases coolant flow is blown-off into the main passage instead of being pulled into the tip gap. This study looks at both the external cooling and flow effects of the microcircuit geometry in the tip region.

One of the first exercises performed was a comparison of the microcircuit and dirt purge coolant flow distributions calculated by Pratt and Whitney to the computational calculations presented in this thesis. The comparison showed the coolant flow distribution among the microcircuit and dirt purge holes to remain relatively constant at the four experimental cooling levels of 0.5%, 1.0%, 1.5% and 2.0% that were examined.

This was due in part because the pressure distribution around the blade remained constant for all tests. Shown in Figure 5.24 is a comparison of the flow distribution predicted by Virginia Tech simulations to those calculated by Pratt & Whitney [Praisner, 2002]. Relatively good agreement is seen between the results with the most noticeable variations occurring for the dirt purge. In all other locations the flow distribution appears to match well enough and does not suggest any unusual results. As expected, more flow exits the five ducts in the leading edge with those being larger than the others, while the flow in ducts 6-16 is constant.

In Figure 5.25, the momentum flux ratio of each microcircuit and dirt purge hole is shown for cases of 1.0% and 1.5% blowing. The momentum flux ratio was based on local injection conditions divided by the upstream fluid conditions and does not vary with tip gap height.

$$I = \frac{\rho_{local} U_{local}^2}{\rho_{inlet} U_{inlet}^2} \tag{5-1}$$

Momentum ratios from the first five jets (1-5) shows a continuous increase in momentum moving from ducts one to five before leveling off and remaining relatively constant for jets 6-15. The final duct shows significantly less momentum than its nearest neighbors with levels close to those seen in the leading edge microcircuits. The two dirt purge holes, 17-18, have the highest momentum jets. Increasing coolant flow from 1.0 to 1.5% results in a more than doubling of the local momentum flux ratios.

Pressure contours along the shroud and tip are shown in Figure 5.26 for a small tip with coolant levels set to 0.5%, 1.0%, 1.5% and 2.0% core flow. For pressure predictions along the shroud one can quickly spot white regions, which are the result of high velocity microcircuit coolant impacting the shroud and creating a pressure zone that exceeds the as defined scale. When these white regions are present the maximum pressures inside and outside of the dirt purge cavity are noted.

A thorough investigation of the shroud images in Figure 5.26 yields no startling differences between these pressure contours and those seen for the dirt purge only flow or baseline cases. Starting with the lowest flow case (0.5%) and increasing the coolant flow

to the highest case (2.0%) leads to an increase in cooling air velocity and more high pressure zones that exceed the color bar. This additional blowing, moving from 0.5% to 2.0% cases seems to also be associated with lower pressures in the mid-chord region, which could be a sign of additional tip leakage or more substantial flow separation. Contours along the pressure side of the blade, in the mainstream passage, closely resemble those seen for baseline flow cases (Figure 5.1 and Figure 5.8) as well as dirt purge only flow (Figures 5.9 and Figure 5.10), but the addition of coolant beyond 1.0% creates contours that are not nearly as smooth. The contour roughness may be the result of a pressure side vortex that will discussed in more detail throughout this section. Contours along the leading edge are similar in magnitude and nature to those seen when there was only dirt purge flow. Also noteworthy, is a significant growth in the high pressure region around the leading edge, which has been extended towards the mid-chord with the addition of microcircuit flow.

Tip pressure contours in Figure 5.26 show lower pressures along the mid-chord as the coolant is increased from 0.5% to 2.0% for a small gap. This region continues to experience a pressure drop with additional cooling as pressure levels drop to $C_p = -12$ to $C_p = -14$ with a flowrate 2.0%. This suggests a possible flow separation and/or high velocity flow in this region that will be explored in future figures. The leading edge shows low pressure zones directly adjacent to the dirt purge, especially for higher flows. High pressures are seen around the blade stagnation zone for all flows, which is a change from the dirt purge only flow in which higher pressures were seen only at the higher flows. Leading edge pressures for a small tip gap with microcircuit flow do not seem to vary considerably when compared to cases in which there was only dirt purge flow, but there is enough variation to notice the effect of the microcircuit on increasing pressures.

Taking a look at the pressure contours for large tip gap and microcircuit configuration in Figure 5.27 we find some variations from the small tip gap cases. Things to observe on the shroud include the reduction of white zones within the contour plots. This stems from the fact that the exhaust gases were introduced to a tip gap three times larger than seem with the small tip gap. Much of the microcircuit film cooling flow is washed out and diluted by the momentum of the tip leakage. The presence of increased tip leakage is present with the large tip gap with the low pressure zones near the

vortex continuing to grow with the ever-increasing coolant levels. We also see the prediction of lower pressures in the mid-chord region as the coolant is increased from 0.5% to 2.0%. The cause of these pressure changes could be from the tip leakage separation, microcircuit coolant or a combination of both, but cannot yet be determined without a more thorough investigation of the flow and thermal fields. The leading edge, again, appears to be dominated by the dirt purge flow, which was also seen with the small tip microcircuit contours.

Studying the tip contours of Figure 5.27 we see the same mid-chord pressure drop with additional coolant as was seen for a small tip gap, but the magnitude has been greatly increased indicating intense cooling flow and/or a large flow separation. The leading edge pressures closely resemble those seen from the large tip dirt purge data.

Examining tip leakage with dirt purge and microcircuit blowing as depicted in Table 5.1 shows that the microcircuit does not reduce the amount of tip leakage when we look at the *CFD* column and compare to baseline cases or cases with dirt purge blowing. For both small and large tip gaps the amount of flow through the tip remains the same as compared to the respective flat tip cases and cases with dirt purge blowing. Instead of hot gases leaking over the tip, the microcircuit does provide significant amounts of cooler air thereby increasing the life of the tip and providing a better operational environment. The prediction of tip leakage appears to be good when looking at *BOAS* ΔP and once again poor for *Tip* ΔP. Looking at Figure 5.3 in which a plane has been placed in the middle of the tip gap for a small and large tip gap with 1.5% blowing shows contours of the non-dimensional velocity magnitude. As seen with the previous cases that have been examined (flat tip and dirt purge blowing), there is a higher tip leakage velocity with a large tip gap, but the according to Table 5.1 the average gap velocity is constant. At both tip gaps there are high and low velocity streaks along the mid-chord that are the result of microcircuit coolant streaking across the blade. The leading edge shows lower velocities that both the dirt purge blowing cases and the flat tip cases.

Figure 5.28a-d shows streamlines that are colored by non-dimensional temperature being released from within the plenum for four cases consisting of two tip gaps with blowing of 1.0% and 1.5%. Significantly more blow-off into the pressure side of the blade is seen when there is a small tip gap (Figure 5.28a and Figure 5.28c) creating

a pressure side vortex. From an aerodynamic standpoint the formation of a pressure-side vortex is undesirable, but if it blocks significant amounts of hot tip leakage flow and keeps the blade cool, it may be worthwhile. As cooling drops from 1.5% to 1.0% with the small tip cases of Figures 5.28a and c there is some decline in the coolants penetration into the mainstream flow, but the blow-off remains high. Only by increasing the size of the tip gap does the blow-off become less noticeable with its near disappearance for a large tip gap and 1.0% blowing of Figure 5.28d. Even when there is blow-off at the large tip, it occurs only in the front most ducts whereas small tip gap blow-off occurred from nearly every microcircuit hole. And while these front ducts (1-5) generally carry more coolant flow than the ducts further back (6-16) their momentum is generally comparable if not lower than the ducts in the mid-chord. It could be that blow-off in the leading edge is partially due to dirt purge flow.

A pressure side plane (PS2) is depicted in Figure 5.29a-b with 1.5% cooling flow for a small and large tip gap, respectively. Contours of non-dimensional temperature and velocity vectors are plotted. In Figure 5.29a there are radical changes from any of the other PS2 planes shown prior, including baseline and dirt purge blowing cases of Figures 5.6 and 5.14. Instead of flow being drawn into the tip gap (located in the upper left region of the plot, $z/S = 0$ and $y/P = 0$) there is substantial microcircuit blowing that somewhat resembles the suction side vortex seen along the SS6 plane. The temperature contours show coolant throughout the entire horizontal span of the plane with spanwise penetration to $z/S = -0.15$, a rather large and significant amount of coolant is passed into the main passage and appears to be wasted. The vortex is centered near $y/P = 0.22$ and $z/S = -0.06$ and appears to be very strong, encompassing a region throughout most of the flow plane.

Figure 5.29b depicts a large tip gap with 1.5% blowing. In the same fashion seen for the small tip case, there is a large amount of cooling air blown-off into the main passage. The coolant penetration into the mainstream at a large tip does not maintain the same size and magnitude that was seen with a small tip. This is due in part because of the increased tip leakage associated with the large gap case, evident by looking at the vector size around $y/P = 0$ and $z/S = 0$ that serves to dilute much of the cooling flow. The vortex is centered near $y/P = 0.0175$ and $z/S = -0.15$ with less circulation and intensity

than the small gap vortex. Also worth noting is the size of the vectors along the blade surface (y/P = 0) which are similar in size to those seen in the small gap case, a considerable change from previous geometries.

The tip leakage vortex is shown in Figure 5.30a-b (SS6) for a small and large tip gap, respectively. The microcircuit and dirt purge cooling level is 1.5%, the same level used to depict the pressure side vortex of Figure 5.29a-b. The tip leakage vortex experiences significant changes with the addition of microcircuit tip cooling. Focusing first on the small gap of Figure 5.29a and comparing it to previous depictions of the SS6 plane in Figures 5.5 and 5.12 it is evident that there are changes in flow patterns along the suction side of the blade. In earlier small tip gap vortices that are shown without a microcircuit, flow is seen to be unaffected by the tip vortex below z/S = –0.2. However, with the addition of the microcircuit the flow throughout the entire region can be seen swirling down along the suction side of the blade, before being pulled away from the blade and back up again. Part of this phenomena may be due to the pressure side vortex that develops and is very strong at the small tip cases, but nonetheless the suction side vortex is larger with microcircuit flow. Its overall position does not change, as it remains around y/P = 0.1 and z/S = -0.05. A cool region is located at the center of the vortex with warmer temperatures in the surrounding bands. Coolant can be seen from the shroud (z/S = 0) to near z/S = -0.10 and throughout the entire y/P range of the plot.

Figure 5.30b shows the tip leakage vortex with a large tip gap. While the small tip and microcircuit appear to increase the size of the vortex, the large tip and microcircuit cooling appear to reduce the vortex. In previous images of the SS6 plane (Figure 5.5 and 5.12), the swirling of flow around the vortex consumed the entire plot, but with the vortex of Figure 5.30b there are negligible effects from the vortex below z/S = -0.25. Temperature contours do show a cooler region near the center of the vortex with increased temperatures in the outlying bands. Overall, the temperatures are reduced from the small gap case because of additional mixing. The position of the vortex remains constant between all previously discussed large gap cases.

Streamlines released upstream of the turbine blade are shown in Figures 5.31a-b for both tip gaps. In Figure 5.31a a microcircuit with 1.5% coolant flow and a small tip gap is shown. This image is similar to those shown earlier in the chapter for baseline and

dirt purge flow cases of Figures 5.4 and 5.11 with streamlines released 1.5 tip gaps below the shroud and colored by spanwise velocity. The streamlines indicate that microcircuit cooling flow has a substantial effect on the flow through the passage. It is important to note that while no lines are seen around the blade this should not be interpreted to mean the microcircuit keeps all of the hot gases away. In fact, there are hot gases in this region, as will be shown with the upcoming adiabatic effectiveness plots, but it does appear the hot gases have been reduced. Comparison of the large and small tip cases show that both are effective at displacing the mainstream flow with the small gap providing superior results. Using these streamlines to judge the leakage vortex shows a smaller vortex for both cases, but not shown in these images is microcircuit coolant that is entrained in the vortex that would certainly lead to larger vortices than what is shown.

Contours of adiabatic effectiveness are shown in Figure 5.32 for a microcircuit and small tip gap. Cooling of the tip appears very streaky along the mid-chord suggesting the flow is moving rapidly, and does not mix with the hot leakage gas in any of the cases. Looking toward the pressure side of the blade with lower coolant flows of 0.5% and 1.0% the coolant streaks maintain a constant thickness throughout their path across the blade, but this is not true for the two higher flows of 1.5% and 2.0% in which thin streaks along the pressure side lead to much thicker coolant streaks along the suction side of the blade. There are two possible explanations for this: the coolant spreads as it travels across the blade or there may be some coolant separation from the blade. In this case, the latter explanation is more sensible because one would expect even coolant spreading over all cases, whereas this particular coolant formation occurs only at the higher flows. Future figures will be presented that show coolant leaving the microcircuit duct and its path through the tip gap. Pressure contours certainly suggest a flow separation and it appears the temperature contours match this. Coolant streaks along the shroud, indicate very cool regions just above the tip, and seem to suggest that coolant exits the blade and interacts with the shroud before it again reaches the tip.

The leading edge of the blade in Figure 5.32 shows poor effectiveness at the 0.5% cooling, but a steady increase in effectiveness occurs with more coolant until the entire area is saturated, indicating a very cool surface temperature with cooling of 1.5%. While the dirt purge only data (geometry 3) showed the inability of the dirt purge to completely

cool the stagnation region, a combination of the dirt purge and microcircuit cooling can accomplish this task. Looking at the tip mid-chord region once again, it also worth noting that there is not an increase in cooling moving from 0.5% to 2.0% cooling. The region appears to maintain the same coolant levels throughout each test. Only around the dirt purge do we see a substantial improvement in cooling with additional coolant. Cooling on the shroud is substantial in most of the cases. On the pressure side of the blade there is considerable blow-off from most of the microcircuit ducts with the exception of the lowest blowing ratio. In most cases the coolant appears to impact the shroud and cool it very well before providing limited cooling along the tip.

Figure 5.33 shows microcircuit and dirt purge cooling with a large tip. These temperature contours show effectiveness around the mid-chord of the tip to remain constant and possibly decline with the addition of coolant. Flow spreading does not appear to be a problem with a larger tip gap as the tip does not exhibit streaks anywhere near those seen in the small tip cases. A significant amount of tip leakage flow mixes out and dilutes the coolant flow making it far less effective with a large gap. In the trailing edge, the final microcircuit duct provides minimal cooling of this area, which differs from the cooling predictions seen with a small tip gap. Around the leading edge, predictions indicate the inability of the coolant to adequately cool this section. While the low effectiveness region does shrink with additional coolant it is not eliminated as was the seen for a small tip gap. Over the remaining parts of the leading edge there is better cooling than what was seen with only dirt purge flow, but overall the results are disappointing. As with the mid-chord of the small tip cases there does not appear to be any cooling benefits with additional microcircuit cooling flow.

Shroud images within Figure 5.33 show a wide variety of cooling effectiveness with the four flows tested. At 0.5% cooling flow, the only cooling over shroud occurs near the dirt purge. Shroud cooling at 2.0% is very substantial and rivals the cooling seen for a small tip. At the 1.0% blowing case there are some unique cooling streaks located on the suction side of the shroud near the mid-chord. This positioning is odd and suggests the flow remains along the surface of the blade before being drawn to the shroud after exiting the tip gap, possibly by the tip leakage vortex. For both tip gaps the shroud shows continued improvements in effectiveness with extra coolant, but this additional

coolant is not seen in some of the areas where it is needed, specifically the mid-chord and trailing edge. One has to think that flow separation in this area has to be very significant to the results as indicated by pressure contours.

A total of eight cases were run with combined microcircuit and dirt purge cooling. All of these cases are displayed in Figure 5.34 with arrows added to the adiabatic effectiveness contours along the tip. These arrows make it possible to locate the position and size of each microcircuit duct along the blade surface. Studying the flow as it exits each hole can be important in determining the effect each duct has on the blade surface. An example of this can be seen with the first microcircuit exit (1), located at the front of the blade, it is the only duct to be located on the suction side of the blade. Looking at this hole for each of the eight cases in Figure 5.34 one can see that it generally appears to provide little cooling to the area just downstream of its exhaust. This does not imply that the hole does not provide cooling somewhere along the blade, but one might question its placement. In the cooler regions that exhibit cooling streaks such as around the mid-chord it is possible to see the coolant path in relation to the microcircuit hole from which it came. All of the coolant in this region can be seen to be swept just downstream of the hole from which it originated. This is not necessarily a bad thing, but something to consider when designing the internal structure of the circuits. Since convection occurs within each internal flow duct of the microcircuit there is the potential for significant cooling to take place inside the blade, making the combination of coolant just downstream of the hole, along the blade surface very effective when combined with internal effects.

A cross-section of the dirt purge is examined in Figures 5.35a-d and 5.36a-d for a small and large tip gap, respectively. Figure 5.35a involves a cross-section through the center of the dirt purge cavity, similar to those presented in Figure 5.17 with velocity vectors and temperature contours. In this particular image (Figure 5.35a) there is a total of 0.5% coolant flow of which approximately 20-25% exits through the dirt purge holes. The dirt purge flow can seen exhausting from the ducts and spreading throughout the region. Near the leading edge, just upstream of the cavity are hot gases that have been inhibited from entering most of the cavity by the cooler purge flow. As coolant flows are

increased from 0.5% to 1.0% (Figure 5.35b) and beyond that in Figures 5.35c-d the coolant simply overwhelms the area and excellent cooling results.

Only upon moving to a large tip gap do the results become more interesting from a thermal standpoint. In Figure 5.36a, which shows 0.5% blowing, the coolant exits the purge holes, but is quickly blown downstream and mixed by the hot tip leakage flows that are swept throughout the region. Increasing the coolant flowrate provides continued improvement in effectiveness results with the coolant eventually reaching the shroud and spreading throughout the cavity and tip gap region when 2.0% blowing (Figure 5.36d) has been used. Comparing the 1.0% and 1.5% cases of Figure 5.36b and c to the dirt purge only cases of Figure 5.17b and d one can see the improvement the microcircuit contribute to this region.

A cross-section through the pressure side of the mid-chord and a microcircuit duct shows some interesting flow features for each of the eight cases that were explored. Velocity vectors and temperature contours are plotted for each case. Figure 5.37a-d shows small tip gap cases for all blowing levels while Figure 5.38a-d shows large tip gap cases. In Figure 5.37a in which the coolant flow is 0.5% we see the cool microcircuit air adhering to the blade surface with no apparent blow-off. Hot gases are along the shroud with cooler gases along the tip surface. Increasing the blowing to 1.0% as in Figure 5.38b shows that hot gases in the tip gap have been removed while there is some small, but noticeable blow-off into the main passage. Adding additional flow beyond this level appears to only add flow to the pressure side vortex and allow hotter gases to work in under the cooler flow. This is clearly evident in Figure 5.37d along the tip surface, which was previously cooled very well at 1.0% blowing, but has experienced lesser cooling at 2.0% blowing.

Figure 5.38a-d has similar findings to those seen in Figure 5.37a-d. Starting with a low flow of 0.5% in Figure 5.38a it is clear that cool flow leaves the microcircuit hole before being drawn into the tip gap. Increasing the coolant to 1.0% seems to improve cooling, but there is still a hot region along the tip surface that the coolant has not been interacting with. Adding coolant beyond 1.0%, shown in Figures 5.38c-d for 1.5% and 2.0% cooling, respectively, does not provide any added effectiveness. In fact, the high temperature region on the tip surface grows and the recirculation of flow is clear with the

velocity vectors. This separation zone appears to grow with microcircuit flow and velocity.

Figures 5.39-42 involve pitchwise-averaged adiabatic effectiveness data along the tip and shroud for all eight microcircuit blowing cases examined. Similar data has been presented for dirt purge only cooling in Figures 5.18-21 and should be referenced for additional comparisons. Effectiveness has been averaged along the tip for a small tip case with all four blowing levels in Figure 5.39 with $x/B_x = 0$ being the blade stagnation point and $x/B_x = 1$ being the trailing edge. The first thing to notice is the lack of variation in all four cases from $x/B_x = 0.5$ through $x/B_x = 0.1$. Additional coolant does nothing to improve effectiveness in this region. There are, however, improved results around the leading edge when compared to dirt purge only flow. The microcircuit provides additional coolant when comparing to the dirt purge only cooling cases of Figure 5.18. Cooling effectiveness improves as the blowing of coolant is increased

For a large tip gap with microcircuit blowing as shown in Figure 5.40 there is once again no benefit in effectiveness by adding coolant from $x/B_x = 0.5$ through $x/B_x = 1$. The leading edge does see some improvement when cooling levels are raised to 1.5% after relatively constant cooling with 0.5% and 1.0% blowing levels. While still not reaching levels seen with the small tip gap, the combined microcircuit and dirt purge flow provides adequate cooling when compared to the data shown in Figure 5.19 showing a large tip gap and dirt purge only flow.

Figure 5.41 has shroud pitchwise-averaged adiabatic effectiveness for a small tip gap. Cooling extends beyond the stagnation point for blowing levels at or above 1.0% and continues along parts of the shroud through $x/B_x = 0.5$. Each curve is separated by approximately $\Delta\bar{\eta} = 0.1$ until reaching the trailing edge where $x/B_x = 0.8$ and all the curves begin to collapse due to flow mixing. For large tip gaps as seen in Figure 5.42 the same trends shown with a small tip continue for a large tip. Cooling is seen upstream of the stagnation point for all cases except the 0.5% blowing. There is a relatively constant distance of $\overline{\Delta\eta} = 0.1$ separating the respective curves until x/B_x approaches 1 and the curves begin to converge.

All of the microcircuit data presented in Figures 5.39-42 have been condensed into a final plot that show area-averaged effectiveness plotted against the coolant mass

flow rate in Figure 5.43. The four curves represent the tip with a large and small tip gap and the shrouds with a large and small tip gap. Each of the curves shows a linear progression of cooling effectiveness, unlike the dirt purge only cooling of Figure 5.22. Discussed throughout the section, the small tip gap effectiveness always outperforms the large tip gap. This is particularly evident along the tip where the curves for the large and small tip gap are separated by $\overline{\Delta\eta} = 0.2$, whereas the cooling along the shroud is very similar. With the same amount of coolant released in the small and large tip tests one has to wonder why there are poorer results with a large gap. It looks as if additional tip leakage flow at the large tip gap simply dilutes much of the cooling effectiveness that would otherwise be used along the tip surface.

The concept of internal microcircuits with external film cooling proved to be an interesting concept. Results from this study showed that the current design provides relatively good external cooling over much of the blade with the exception of the trailing edge. While the addition of dirt purge blowing did affect the flow field, these effects were not nearly as significant as those seen with the addition of the microcircuit. An interesting aspect of this research that was unexpected occurred around the mid-chord in which both the large and small tip gaps did not experience a substantial increase in effectiveness with additional coolant. This same trend did not hold around the leading edge where additional coolant served to provide greater cooling capabilities. The amount of tip leakage was generally unaltered by the microcircuit and dirt purge as it appears that tip gap leakage is a function of only the height of the gap. One other phenomena of interest was the formation of a pressure side vortex from microcircuit blow-off.

Table 5.1. Tip gap leakage measurements.

Geometry	Tip Gap Size	Coolant % core flow	BOAS ΔP % core flow	Tip ΔP % core flow	CFD % core flow	BOAS % Diff w/CFD	Tip % Diff w/CFD
Flat	Small	0.00	1.3	1.5	1.3	1.6	13.2
DP	Small	0.19	-	-	1.3	-	-
DP	Small	0.29	-	-	1.2	-	-
Micro/DP	Small	0.50	1.3	1.5	-	-	-
Micro/DP	Small	1.00	1.2	1.5	1.2	0.3	18.4
Micro/DP	Small	1.50	1.2	1.5	1.3	5.6	13.3
Micro/DP	Small	2.00	1.2	1.4	-	-	-
Flat	Large	0.00	3.8	4.7	3.9	3.8	18.7
DP	Large	0.19	-	-	3.9	-	-
DP	Large	0.29	-	-	3.9	-	-
Micro/DP	Large	0.50	3.8	4.7	-	-	-
Micro/DP	Large	1.00	3.8	4.8	3.9	1.2	25.6
Micro/DP	Large	1.50	3.7	5.0	3.8	3.6	30.5
Micro/DP	Large	2.00	3.5	5.1	-	-	-

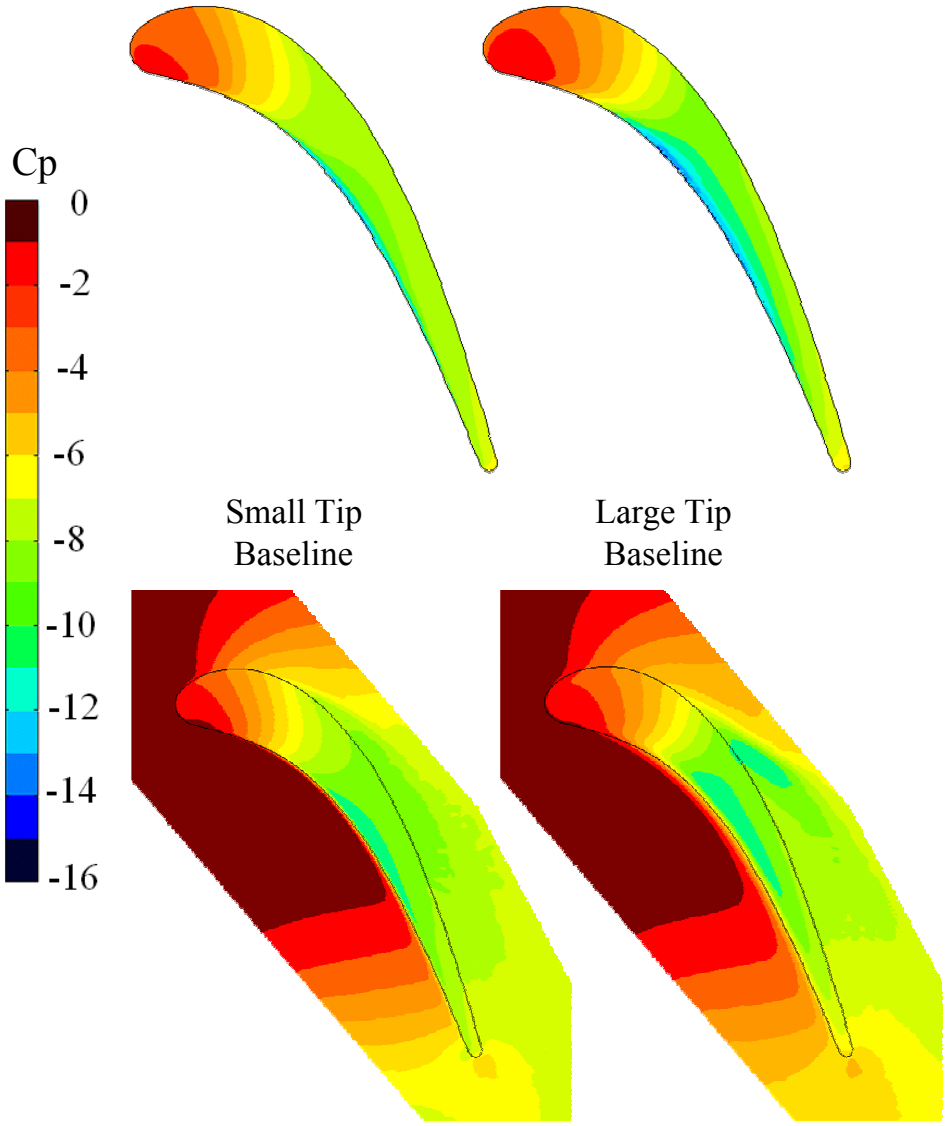

Figure 5.1. Predicted pressure contours along the blade tip and shroud for a flat tip blade with no blowing for small and large tip gaps.

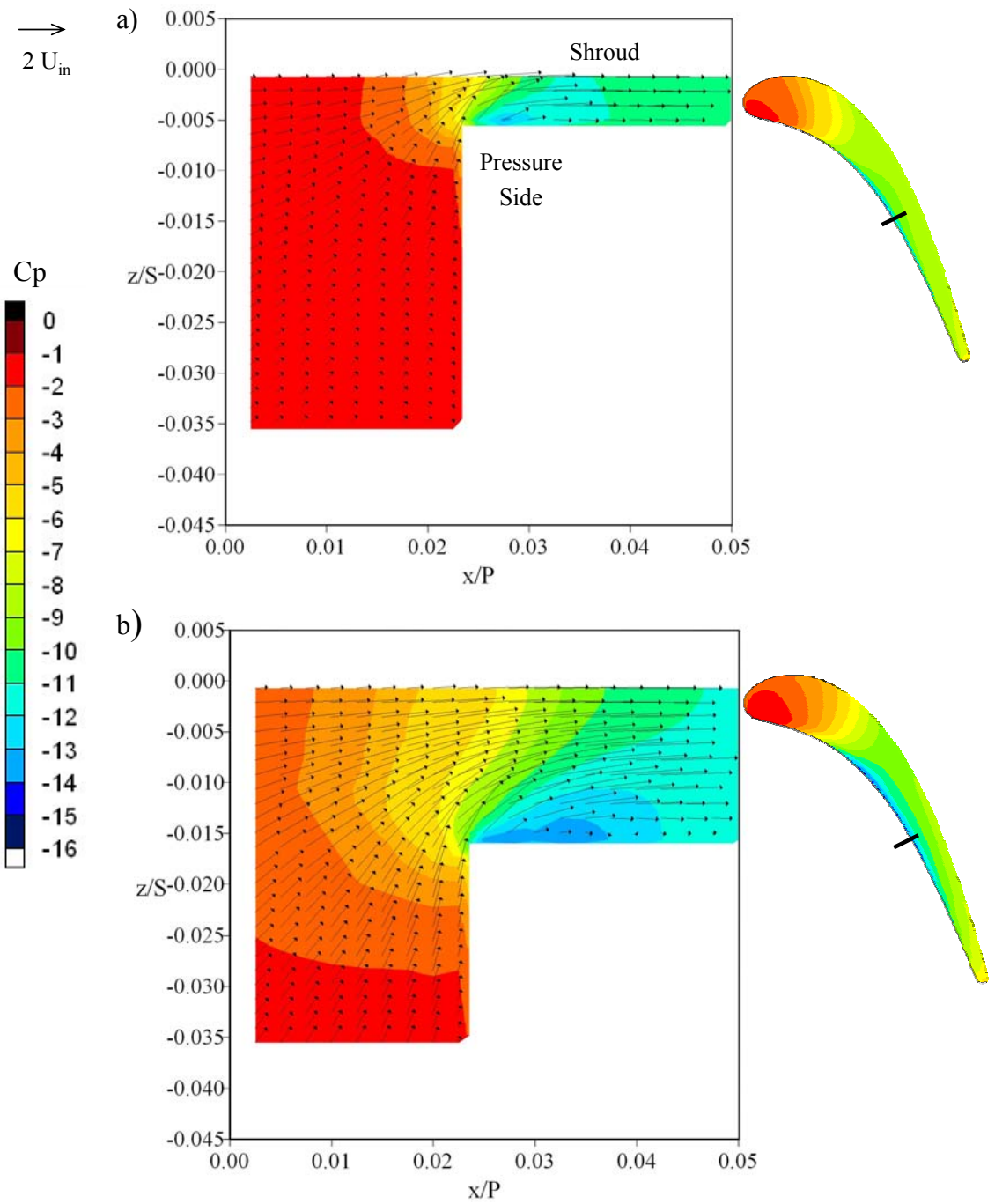

Figure 5.2a-b. Static pressure distributions and velocity vectors in a plane cut through the tip gap near the mid-chord.

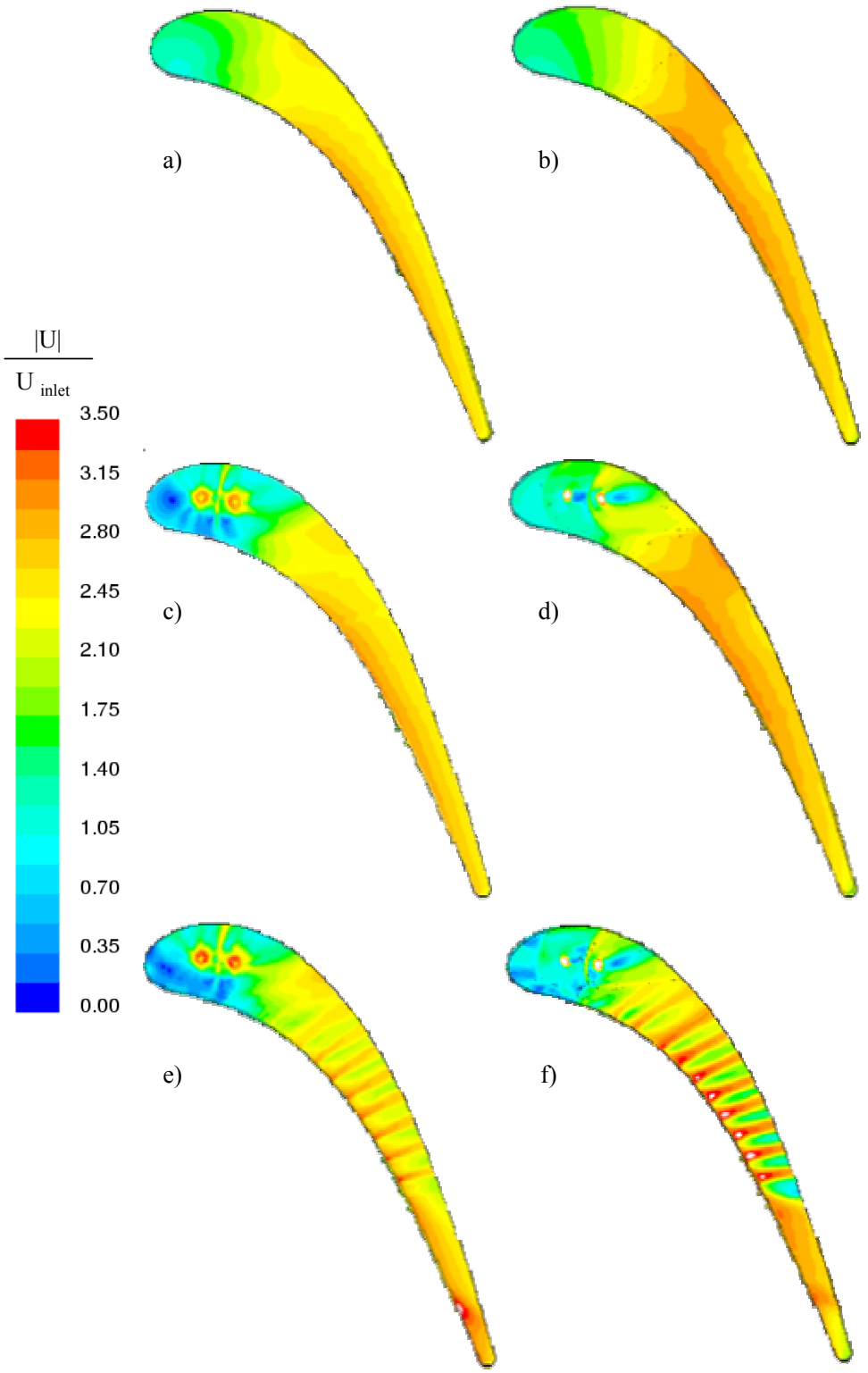

Figure 5.3a-f. Non-dimensional velocity plotted in a plane placed through the middle of a a) small tip gap with a flat tip, b) large tip gap with a flat tip, c) small tip gap with 0.29% dirt purge blowing, d) large tip gap with 0.29% blowing, e) small tip gap with 1.5% microcircuit and dirt purge blowing, and f) large tip gap with 1.5% microcircuit and dirt purge blowing.

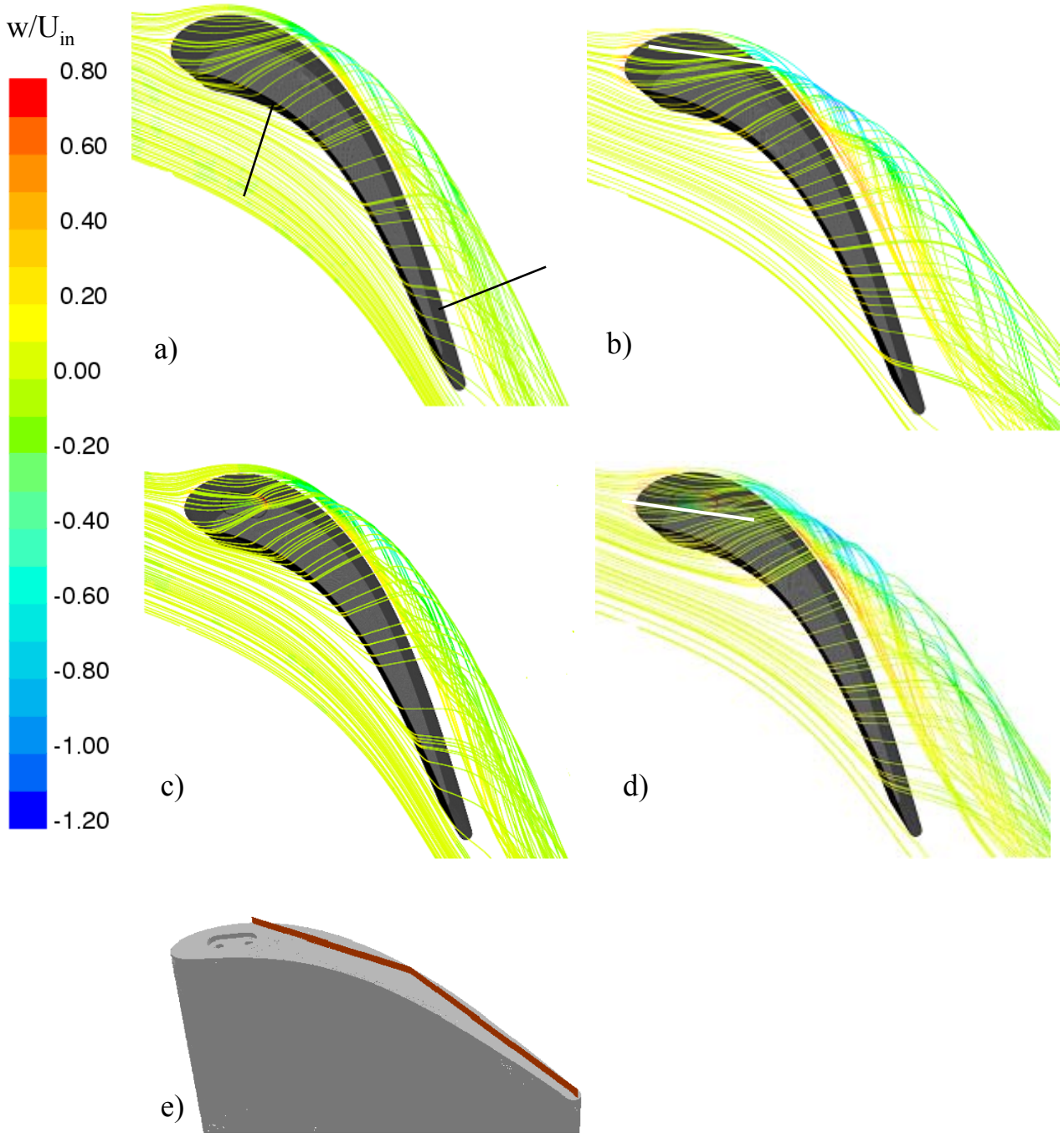

Figure 5.4a-e. Streamlines released from 1.5 tip gap heights below the shroud that are colored by the non-dimensional spanwise velocity component for a) a small tip gap with a flat blade tip, b) a large tip gap with a flat blade tip, c) a small tip gap and non-flowing purge holes, d) a large tip gap and non-flowing purge holes, and e) two planes (red) set-up along the tip to measure tip leakage flow with the placement based on streamlines.

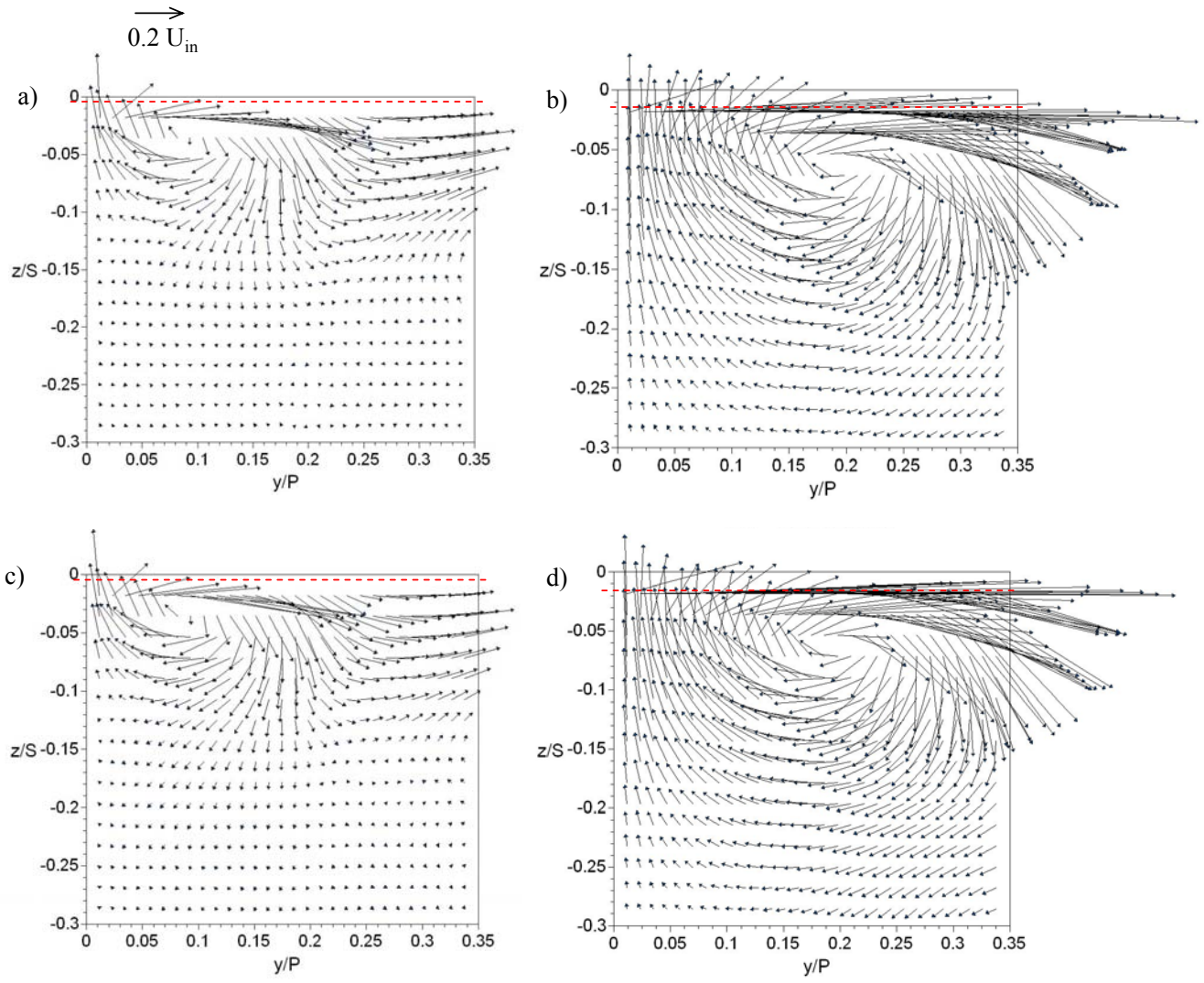

Figure 5.5a-d. Secondary flow vectors along a suction side plane (SS6) defined as being normal to the blade at an axial chord location of 94% for a a) small gap and flat tip, b) large gap and flat tip, c) small gap and non-flowing purge cavity and d) large gap and non-flowing purge cavity.

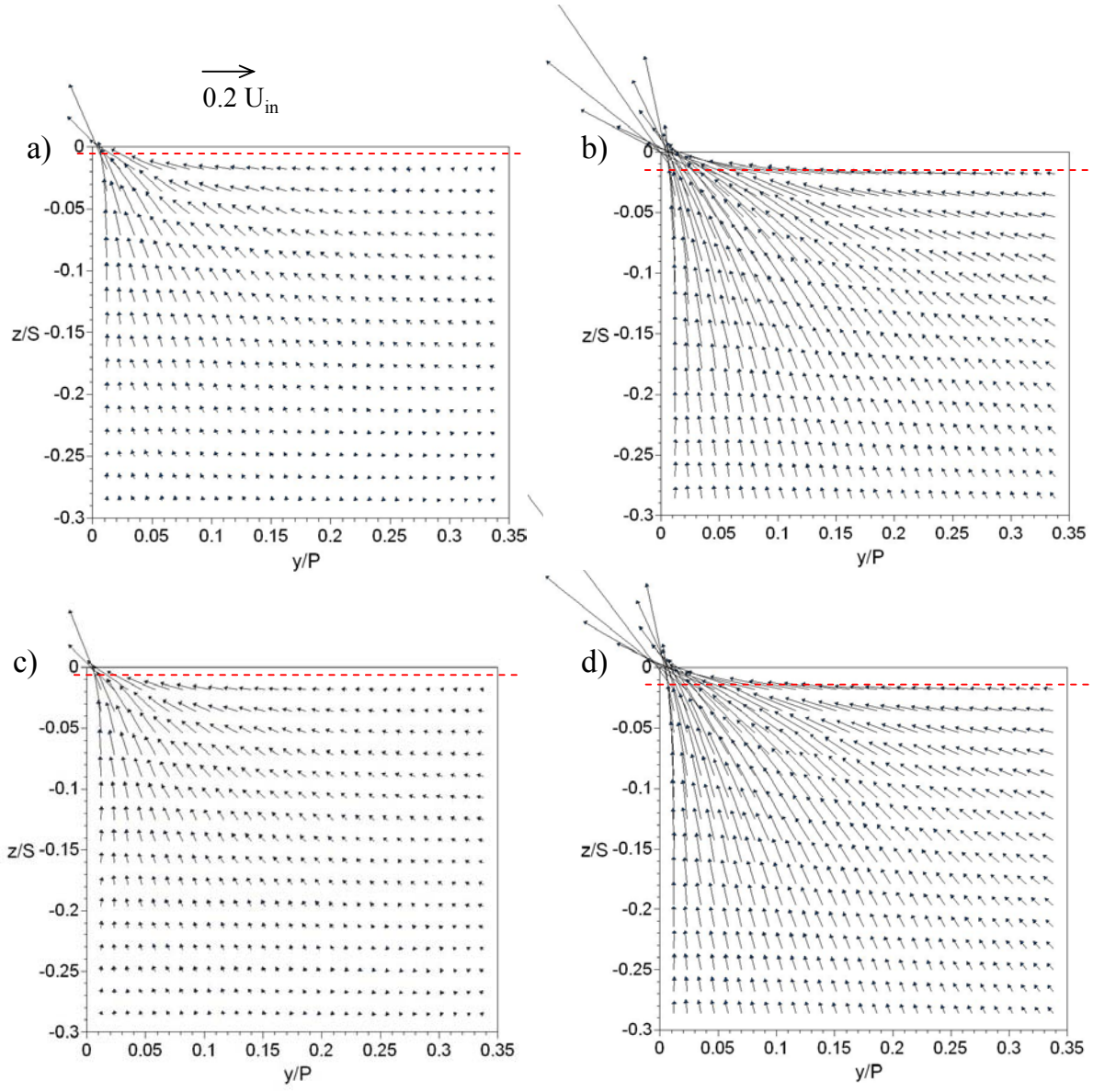

Figure 5.6a-d. Secondary flow vectors along a pressure side plane (PS2) defined as being normal to the blade at an axial chord location of 30% for a a) small tip gap and flat tip, b) large tip gap and flat tip, c) small tip gap and non-flowing purge cavity and d) large tip gap and non-flowing purge cavity.

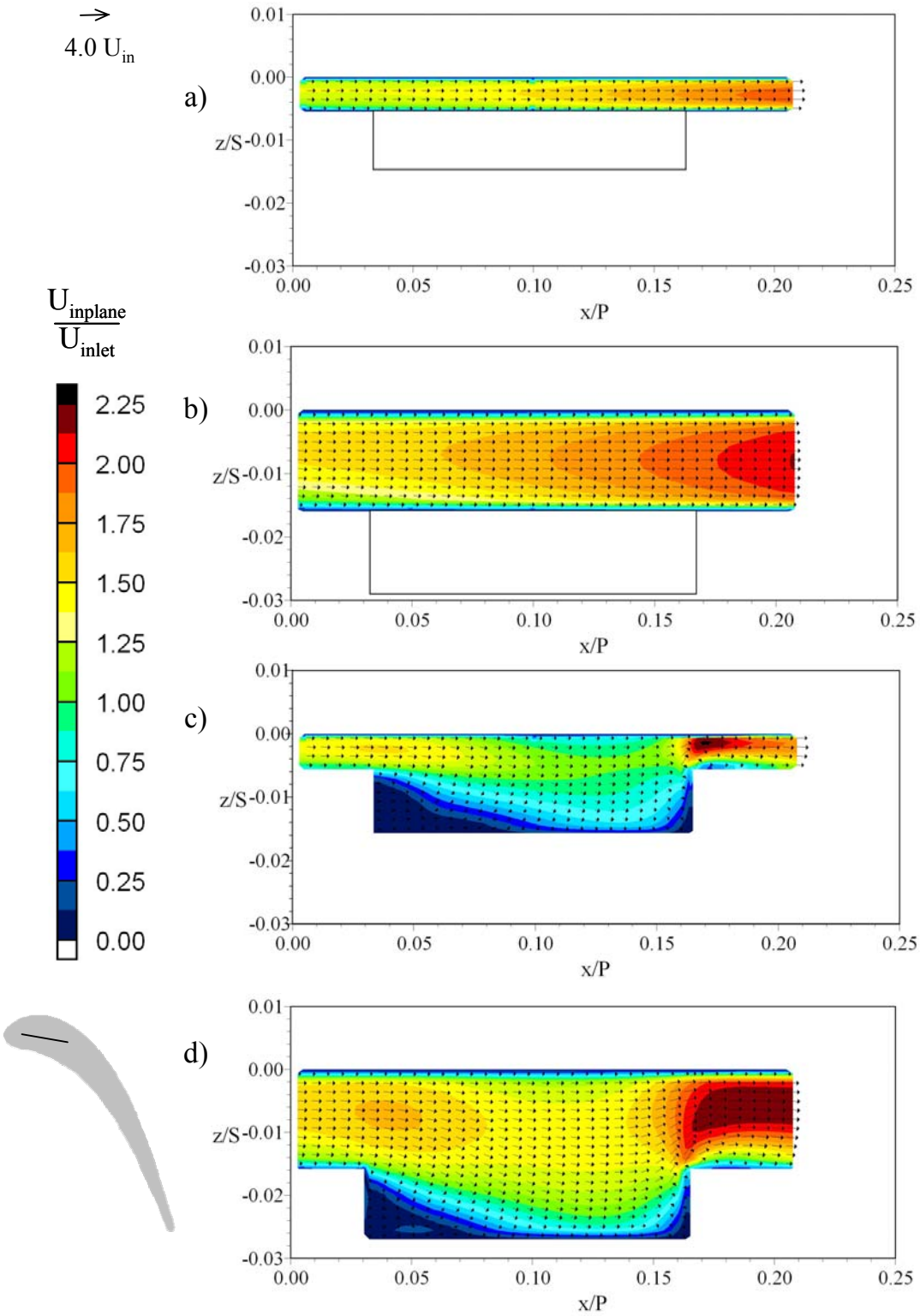

Figure 5.7a-d. Velocity vectors and velocity magnitude shown in a plane cut through the leading edge region of the tip gap where the dirt purge would be located for a a) small gap with flat tip, b) large gap with flat tip, c) small gap and non-blowing dirt purge, d) large gap and non-blowing dirt purge.

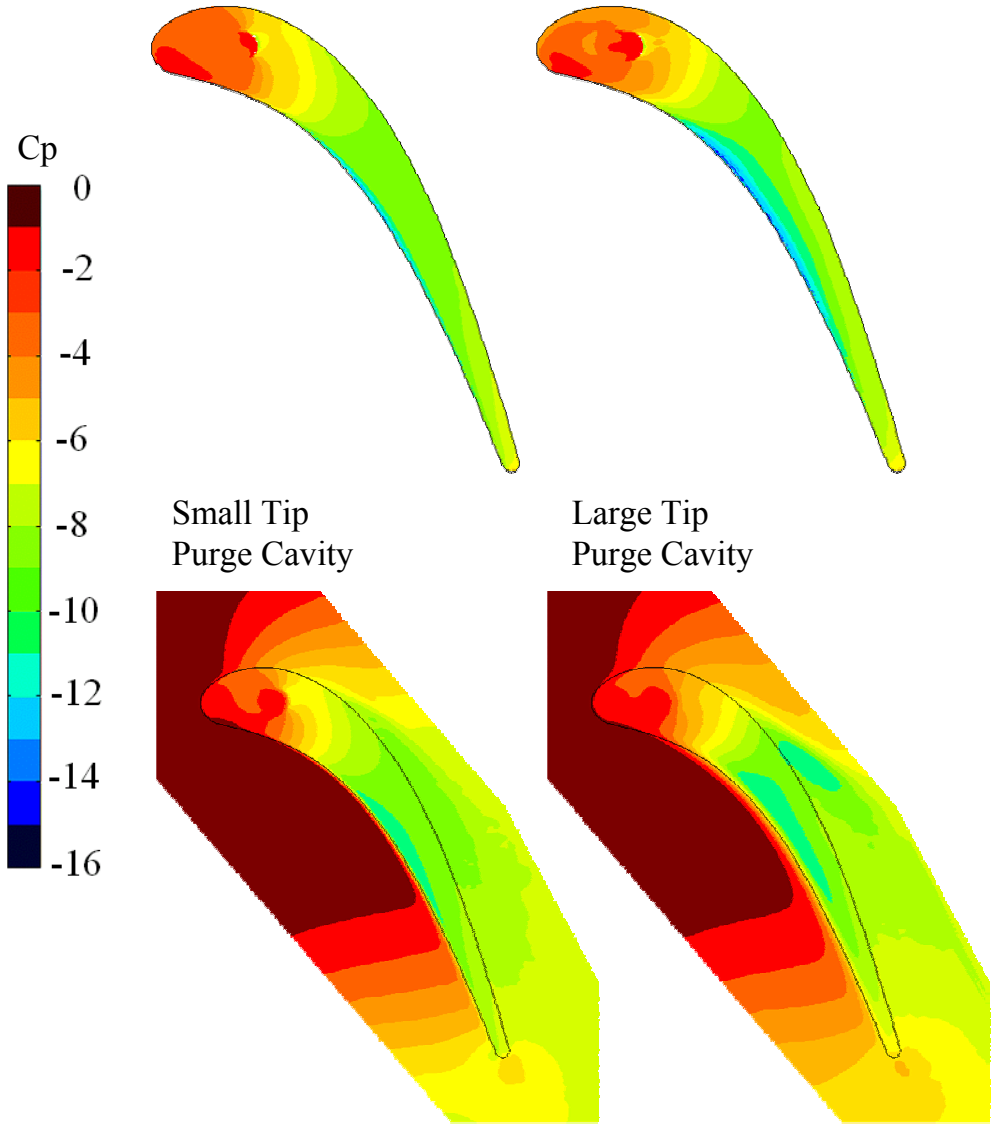

Figure 5.8. Predicted pressure contours along the blade tip and shroud for a non-flowing dirt purge cavity with small and large tip gaps.

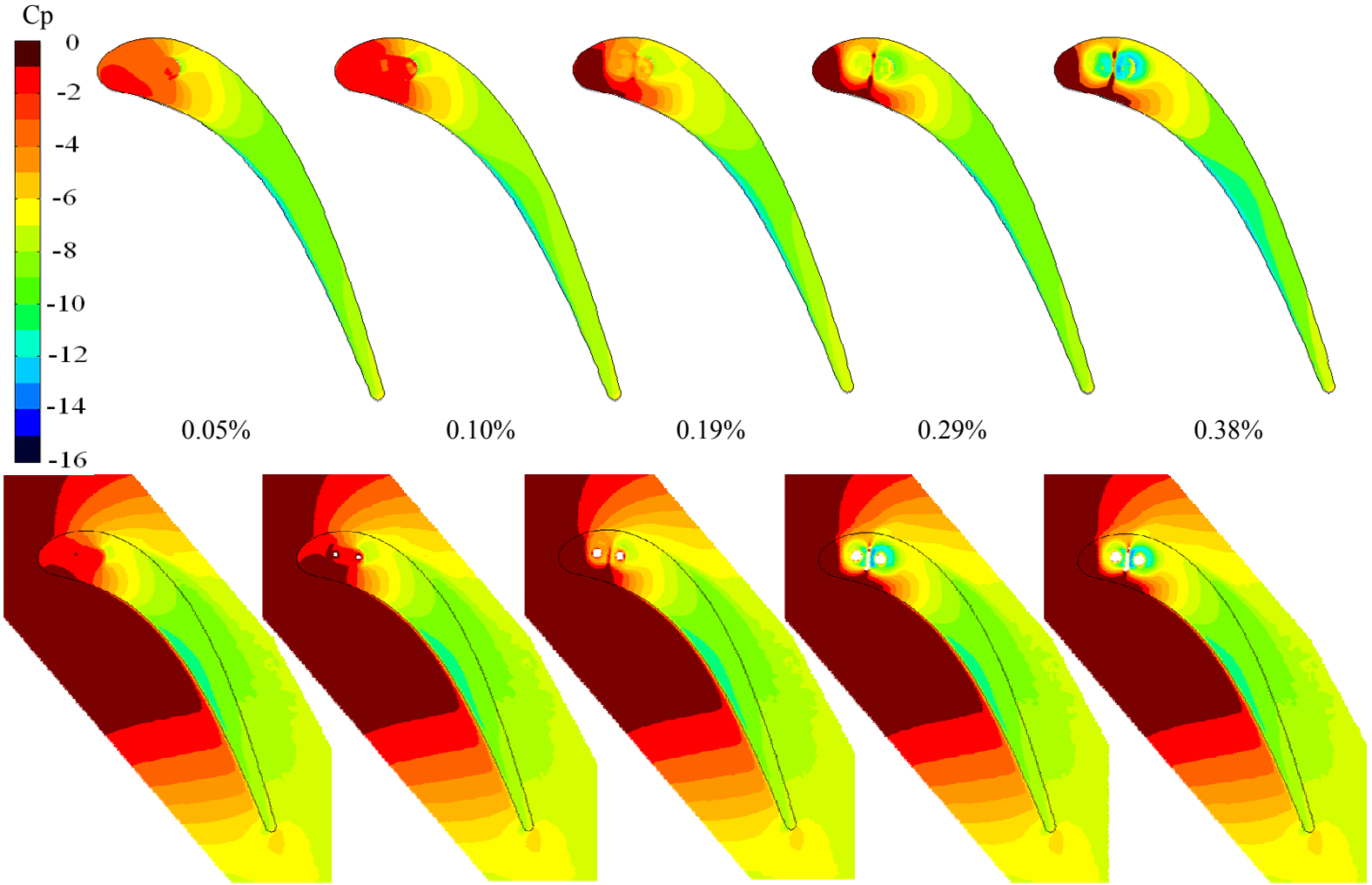

Figure 5.9. Predicted pressure contours along the blade tip and shroud for a dirt purge cavity and small tip gap with blowing ratios of 0.05%, 0.10%, 0.19%, 0.29%, and 0.38% core flow.

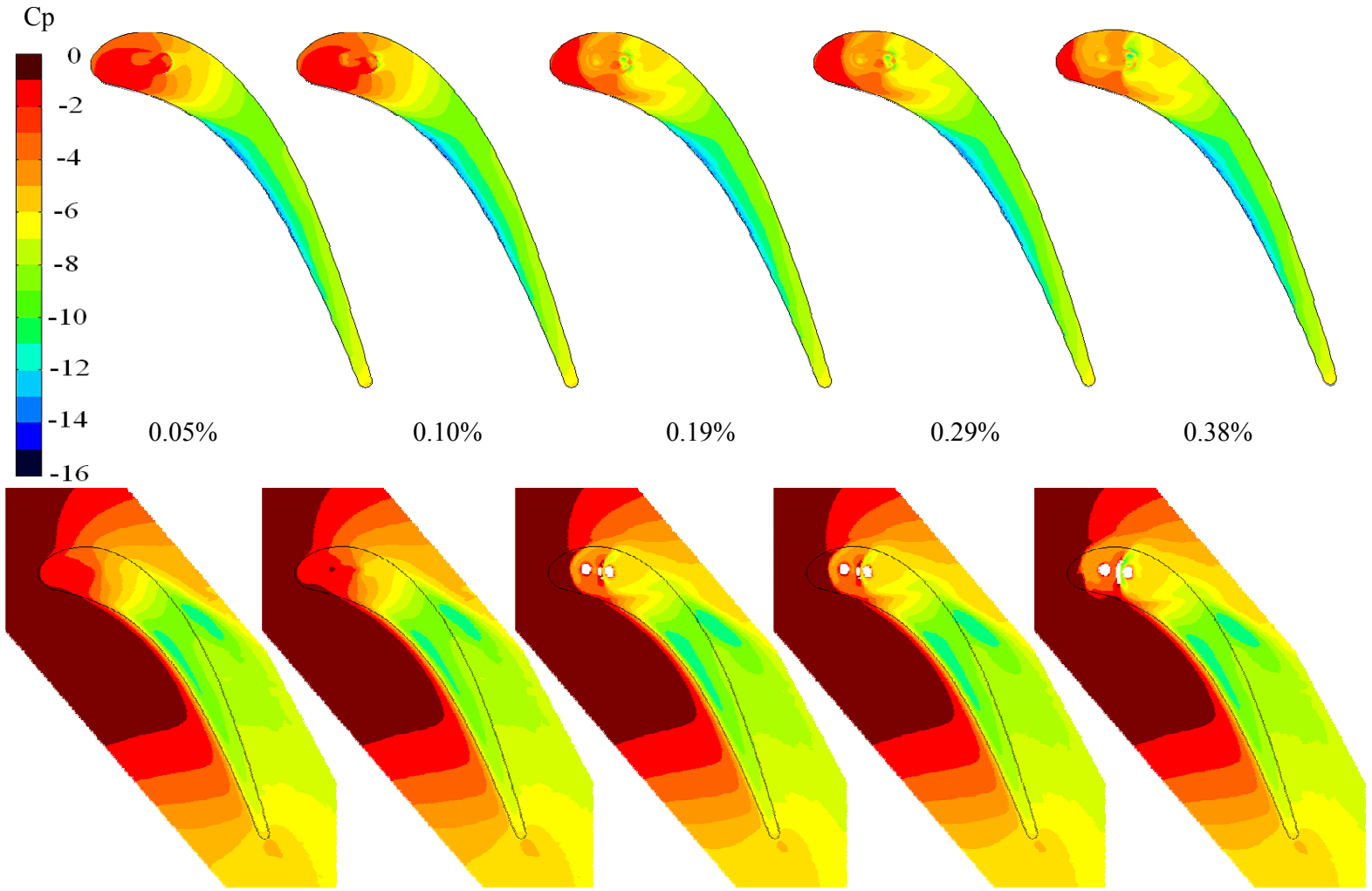

Figure 5.10. Predicted pressure contours along the blade tip and shroud for a dirt purge cavity and large tip gap with blowing ratios of 0.05%, 0.10%, 0.19%, 0.29%, and 0.38% core flow.

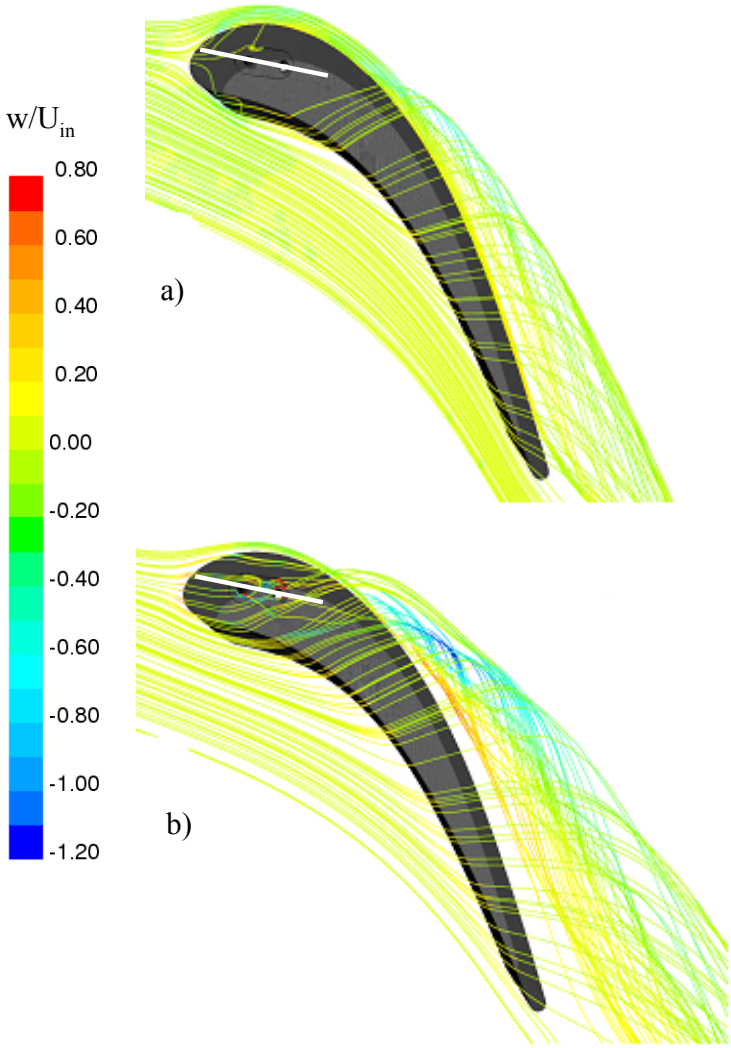

Figure 5.11a-b. Streamlines released from 1.5 tip gap heights below the shroud that are colored by the non-dimensional spanwise velocity component for dirt purge blowing with a a) small tip and 0.29% blowing, and b) large tip and 0.29% blowing.

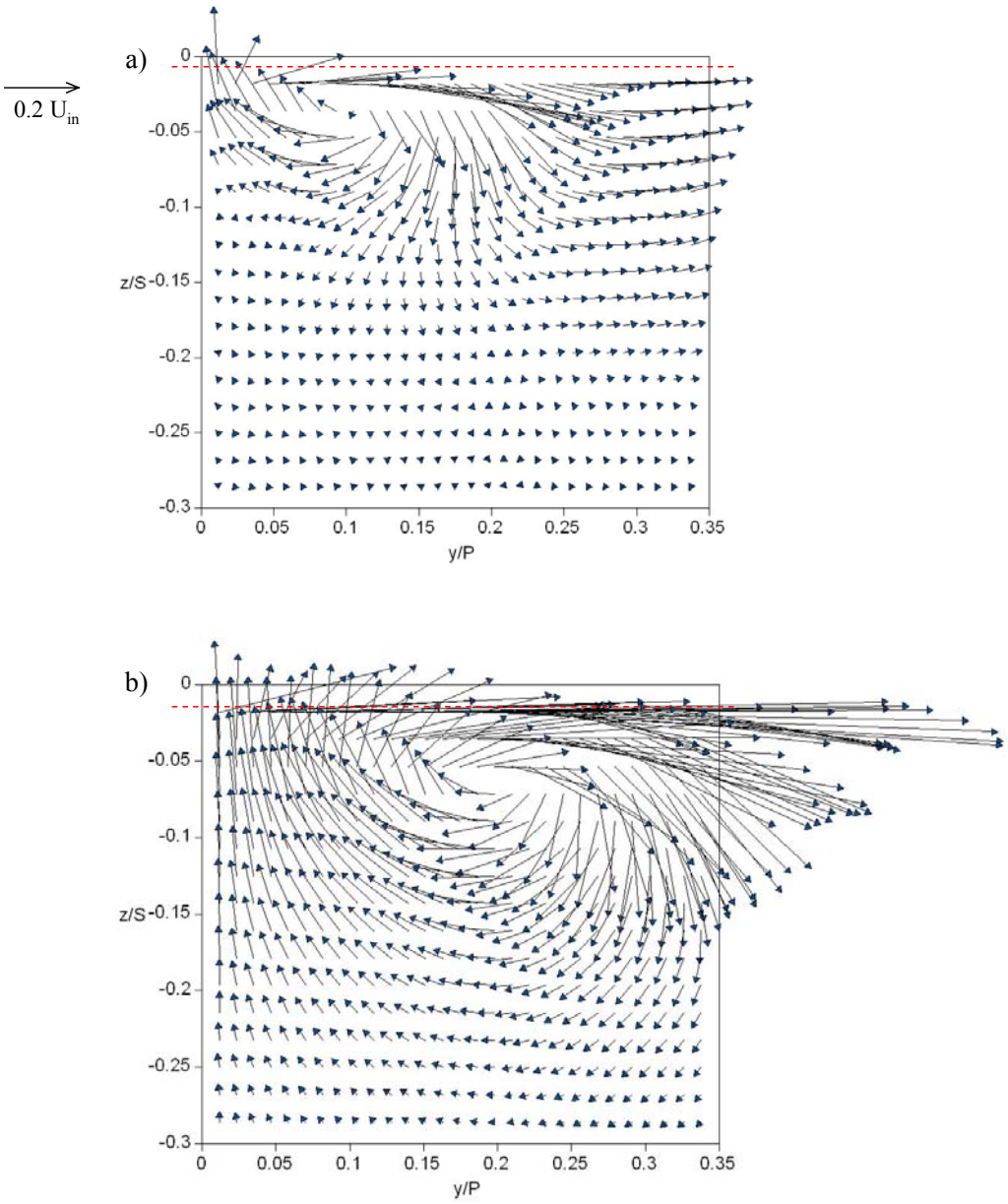

Figure 5.12a-b. Secondary flow vectors along a suction side plane (SS6) defined as being normal to the blade at an axial chord location of 94% for a a) small tip gap and 0.29% blowing, and b) large tip gap and 0.29% blowing.

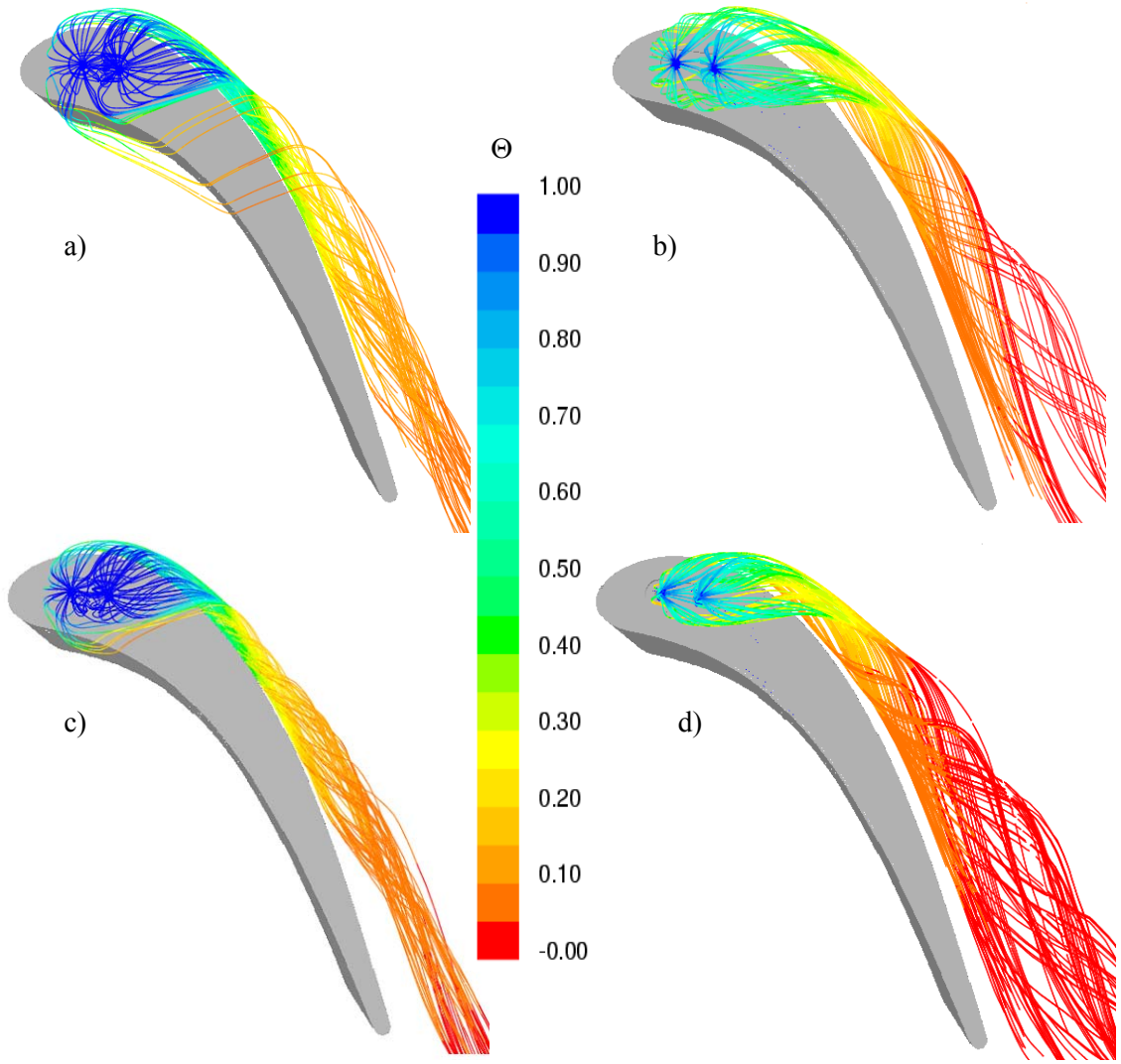

Figure 5.13a-d. Streamlines colored by non-dimensional temperature released from the dirt purge for a a) small tip gap and 0.29% blowing, b) large tip gap and 0.29% blowing, c) small tip gap and 0.19% blowing and d) large tip gap and 0.19% blowing.

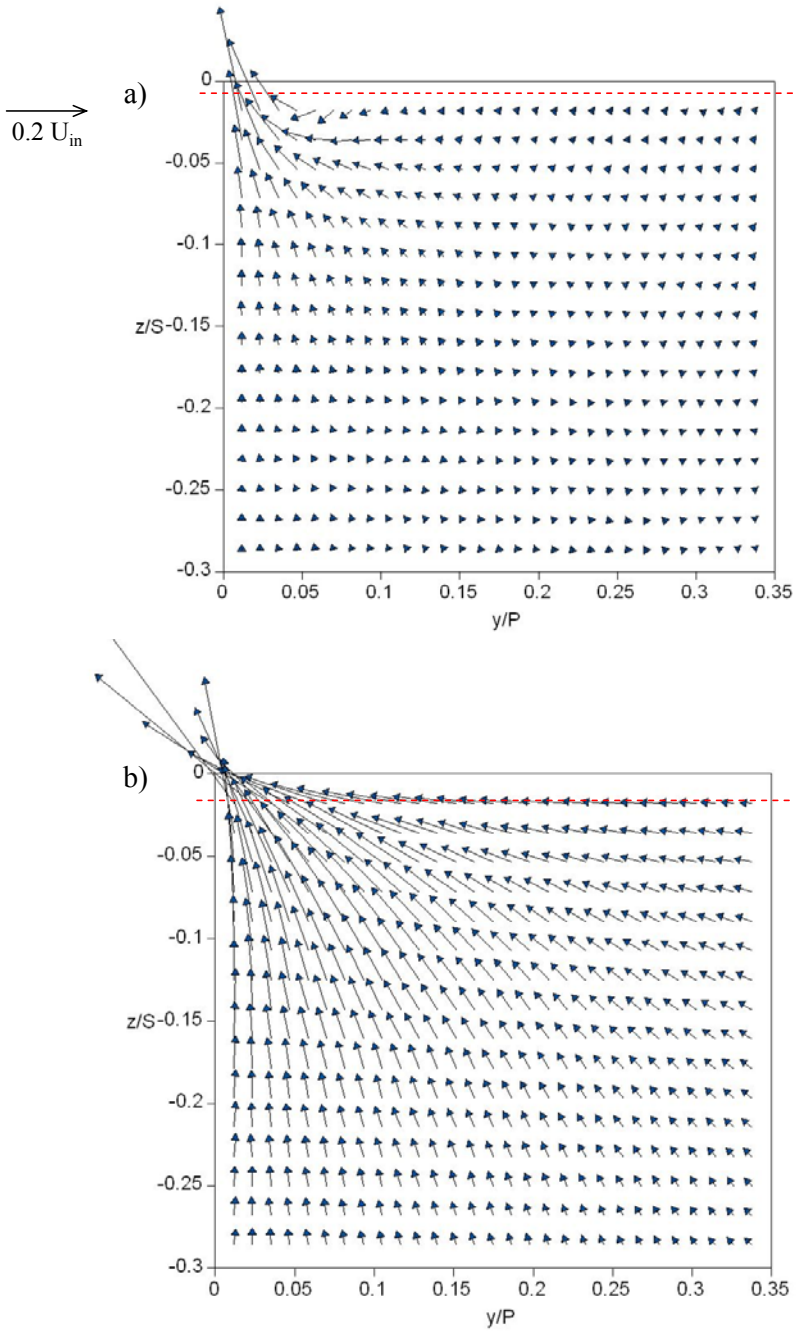

Figure 5.14a-b. Secondary flow vectors along a pressure side plane (PS2) defined as being normal to the blade at an axial chord location of 30% for a a) small tip and 0.29% blowing, and b) large tip and 0.29% blowing.

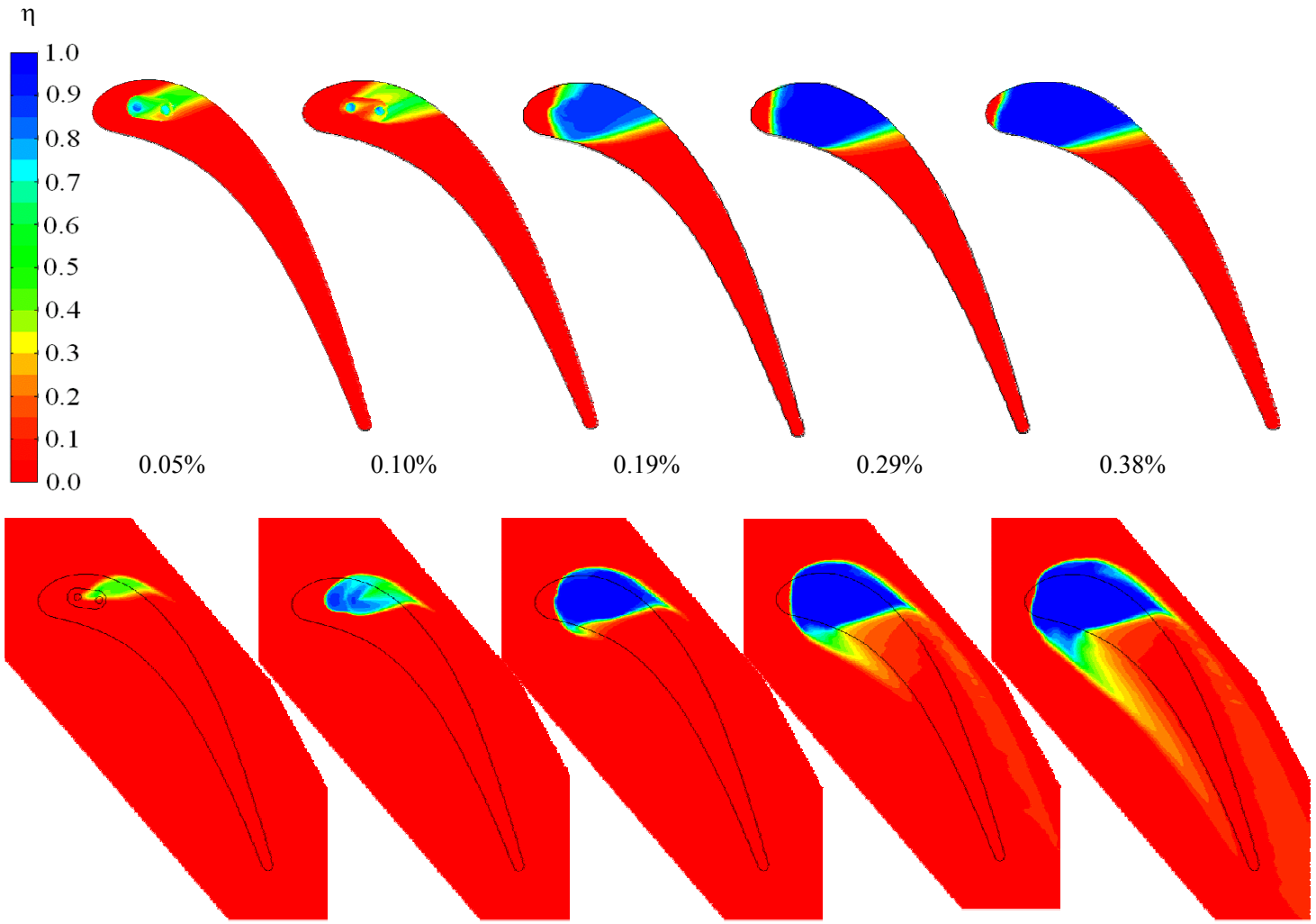

Figure 5.15. Predictions of adiabatic effectiveness along the tip and shroud for the small tip gap with dirt purge blowing at ratios of 0.05%, 0.10%, 0.19%, 0.29%, and 0.38% core flow.

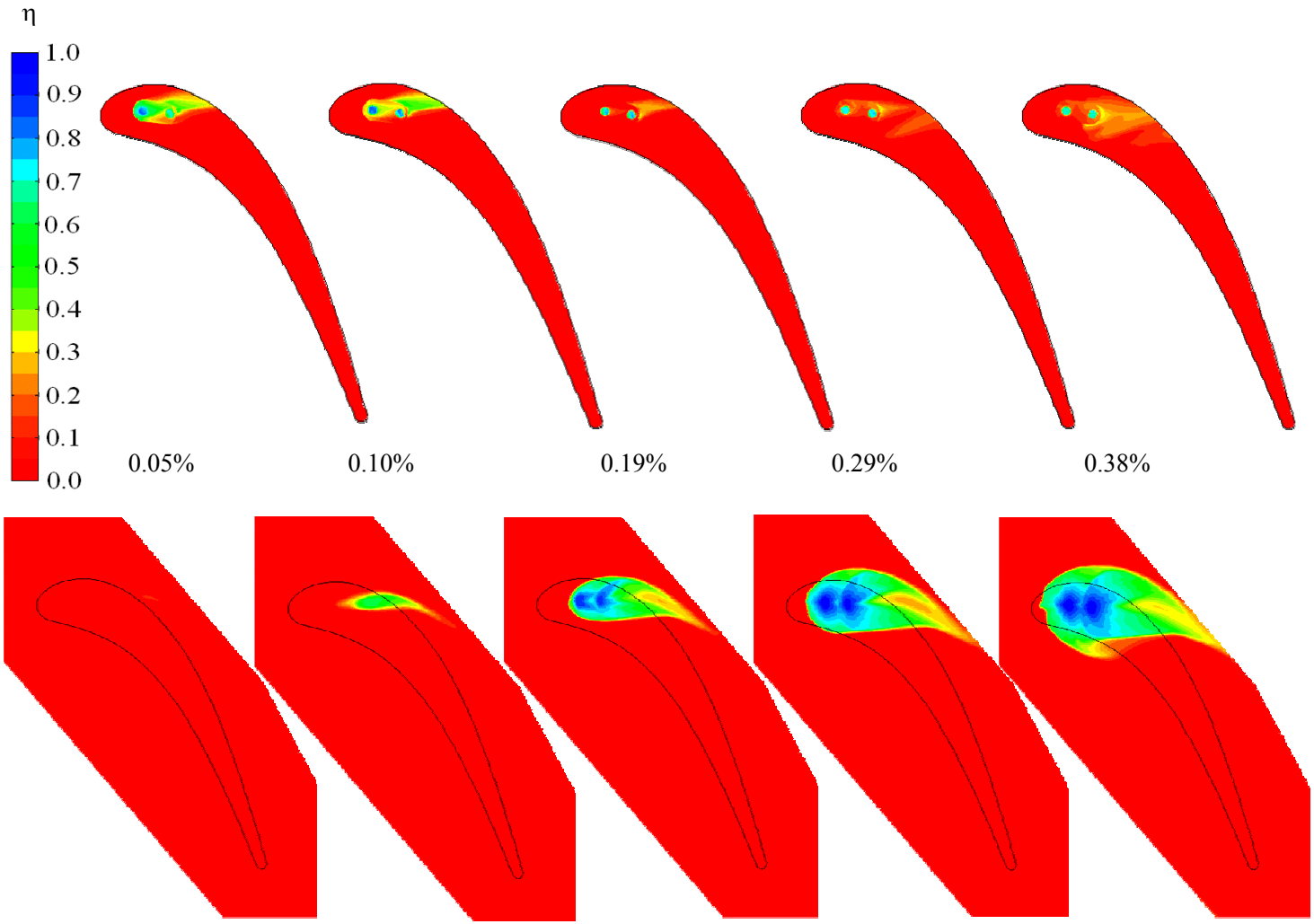

Figure 5.16. Predictions of adiabatic effectiveness along the tip and shroud for the large tip gap with dirt purge blowing at ratios of 0.05%, 0.10%, 0.19%, 0.29% and 0.38% core flow.

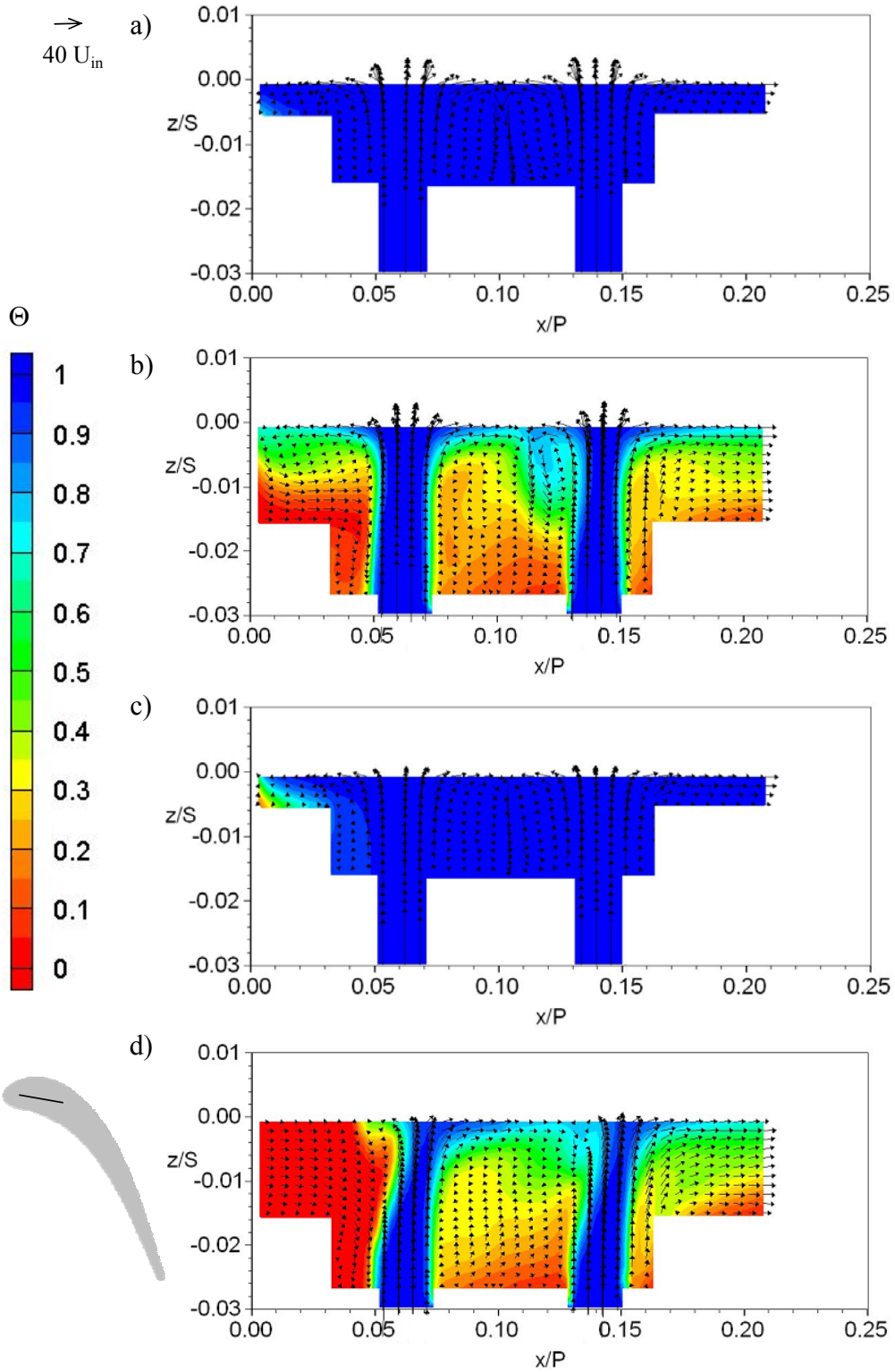

Figure 5.17a-d. Cross-sectional view of the dirt purge for a a) small tip with 0.29% blowing, b) large tip with 0.29% blowing, c) small tip with 0.19% blowing, and d) large tip gap with 0.19% blowing.

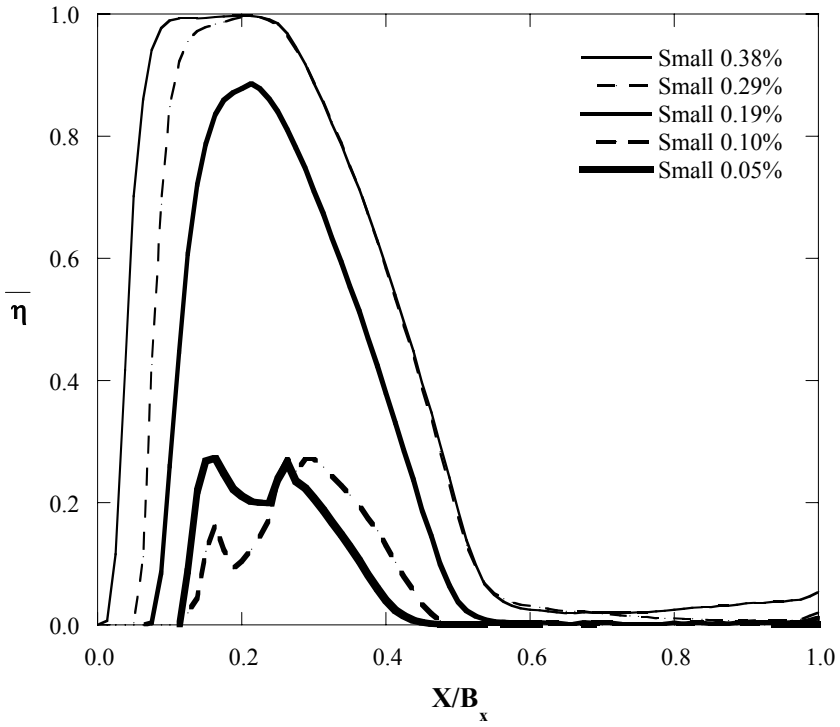

Figure 5.18. Comparison of pitchwise-averaged effectiveness along the tip for the small tip gap with dirt purge blowing.

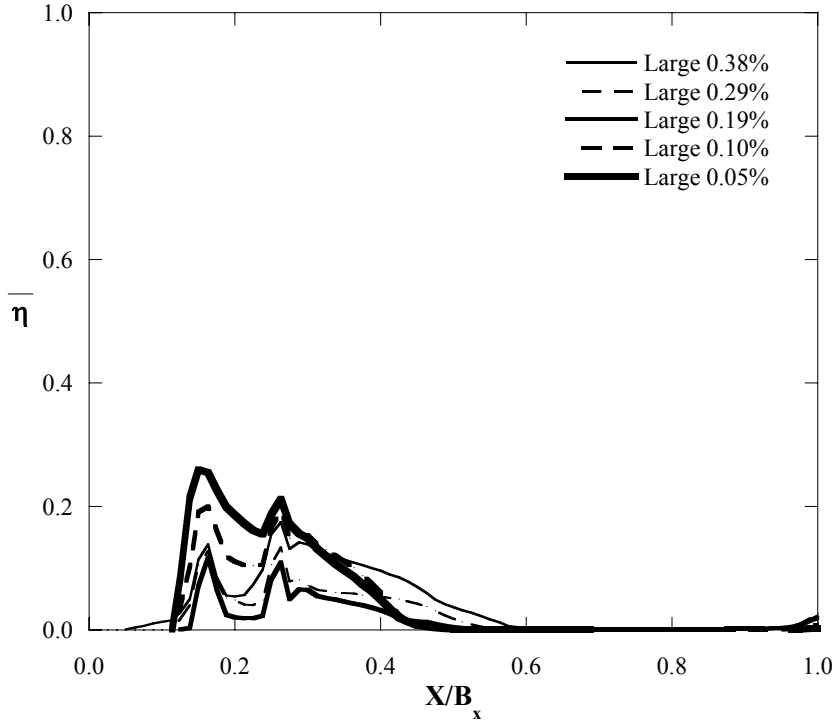

Figure 5.19. Comparison of pitchwise-averaged effectiveness along the tip for the large tip gap with dirt purge blowing.

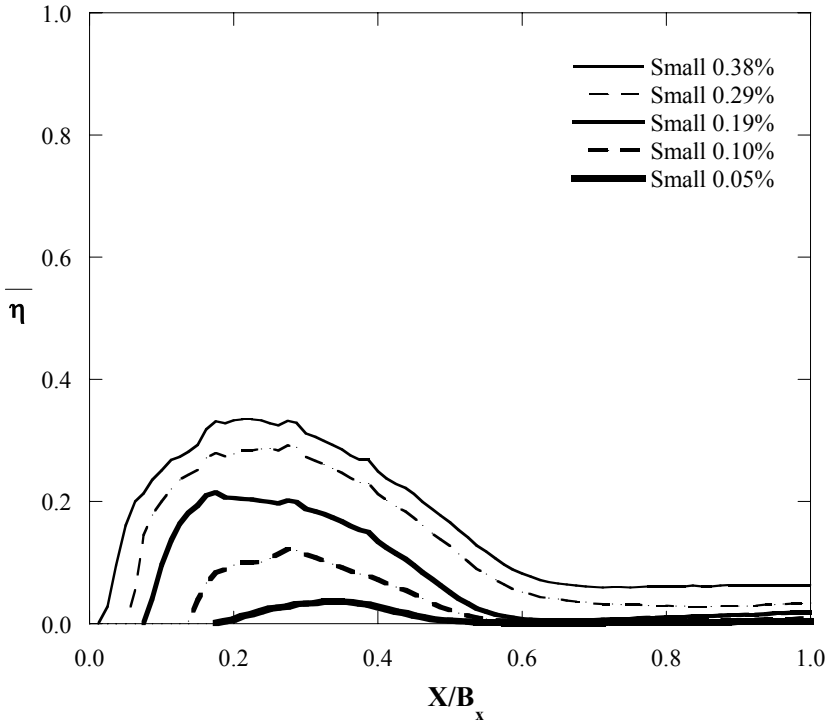

Figure 5.20. Comparison of pitchwise-averaged effectiveness along the shroud for the small tip gap with dirt purge blowing.

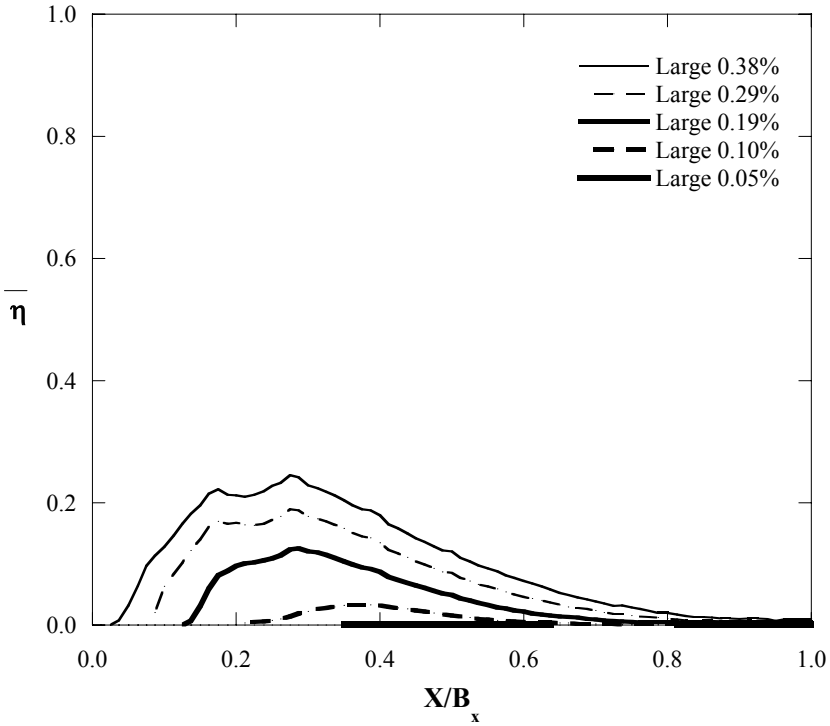

Figure 5.21. Comparison of pitchwise-averaged effectiveness along the shroud for the large tip gap with dirt purge blowing.

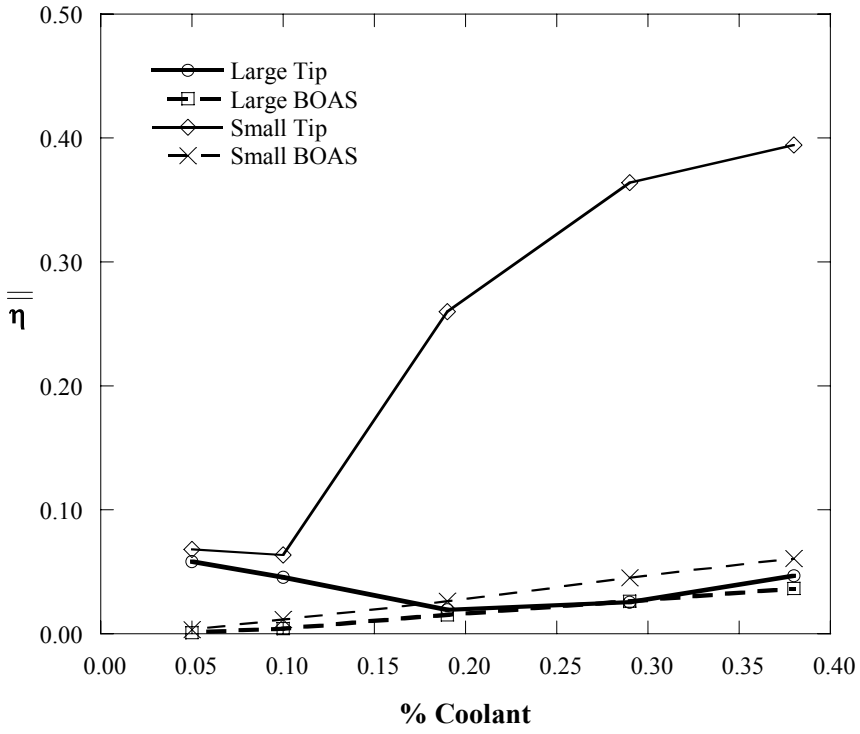

Figure 5.22. Area-averaged effectiveness over the tip and shroud plotted against the dirt purge coolant mass flow rate.

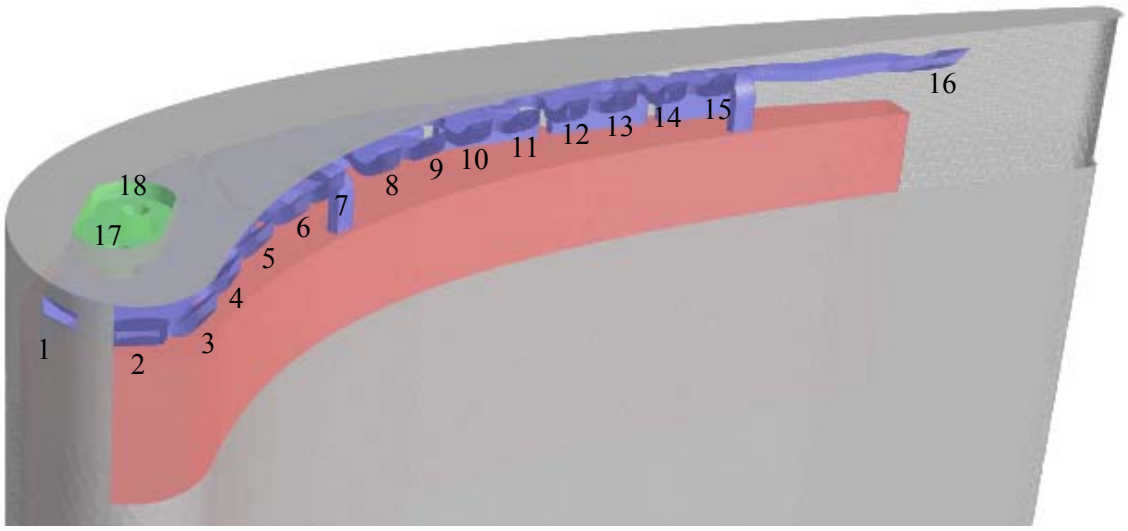

Figure 5.23. Microcircuit and dirt purge numbering scheme.

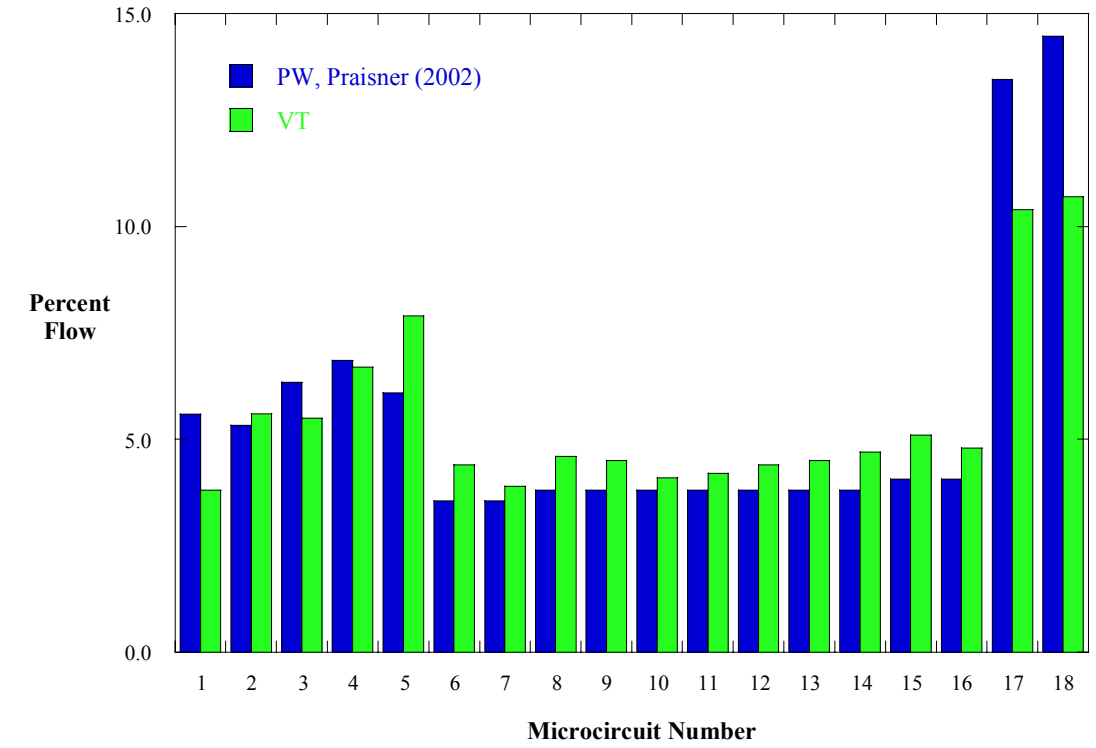

Figure 5.24. Comparison of flow distribution within the microcircuit. Numbers 1-16 represent the microcircuit holes with 17 and 18 the dirt purge holes.

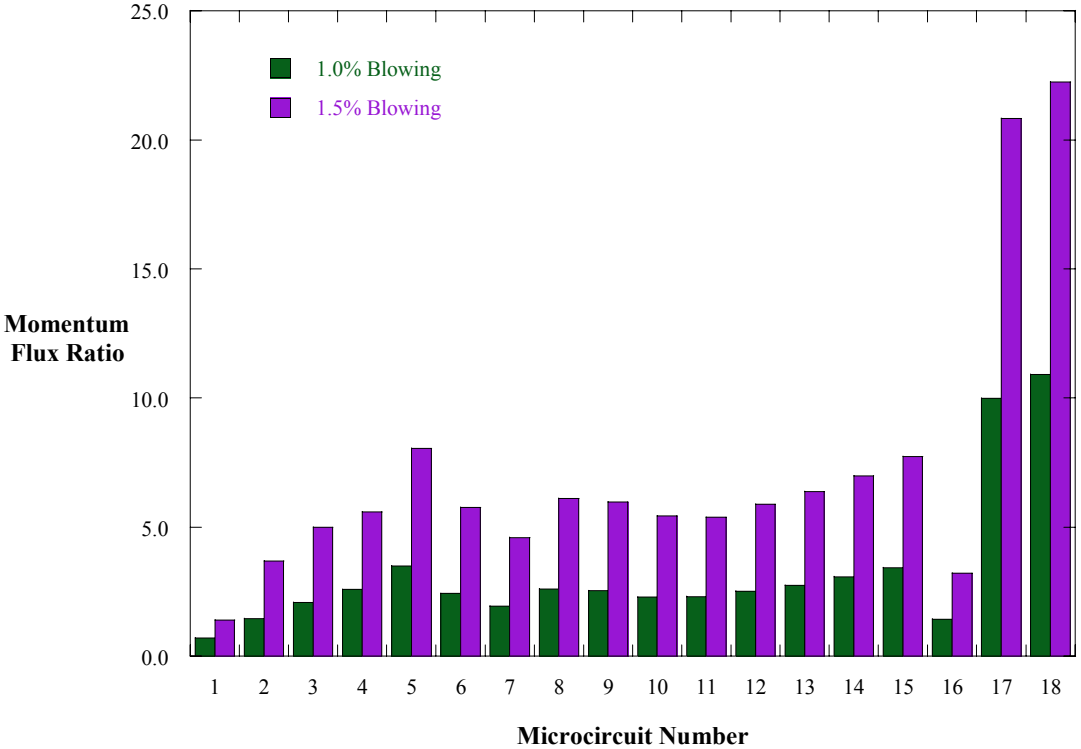

Figure 5.25. Momentum flux ratio for microcircuit cooling ducts at 1.0% and 1.5% cooling flow which is independent of tip gap height. Numbers 1-16 represent the microcircuit holes with 17 and 18 the dirt purge holes.

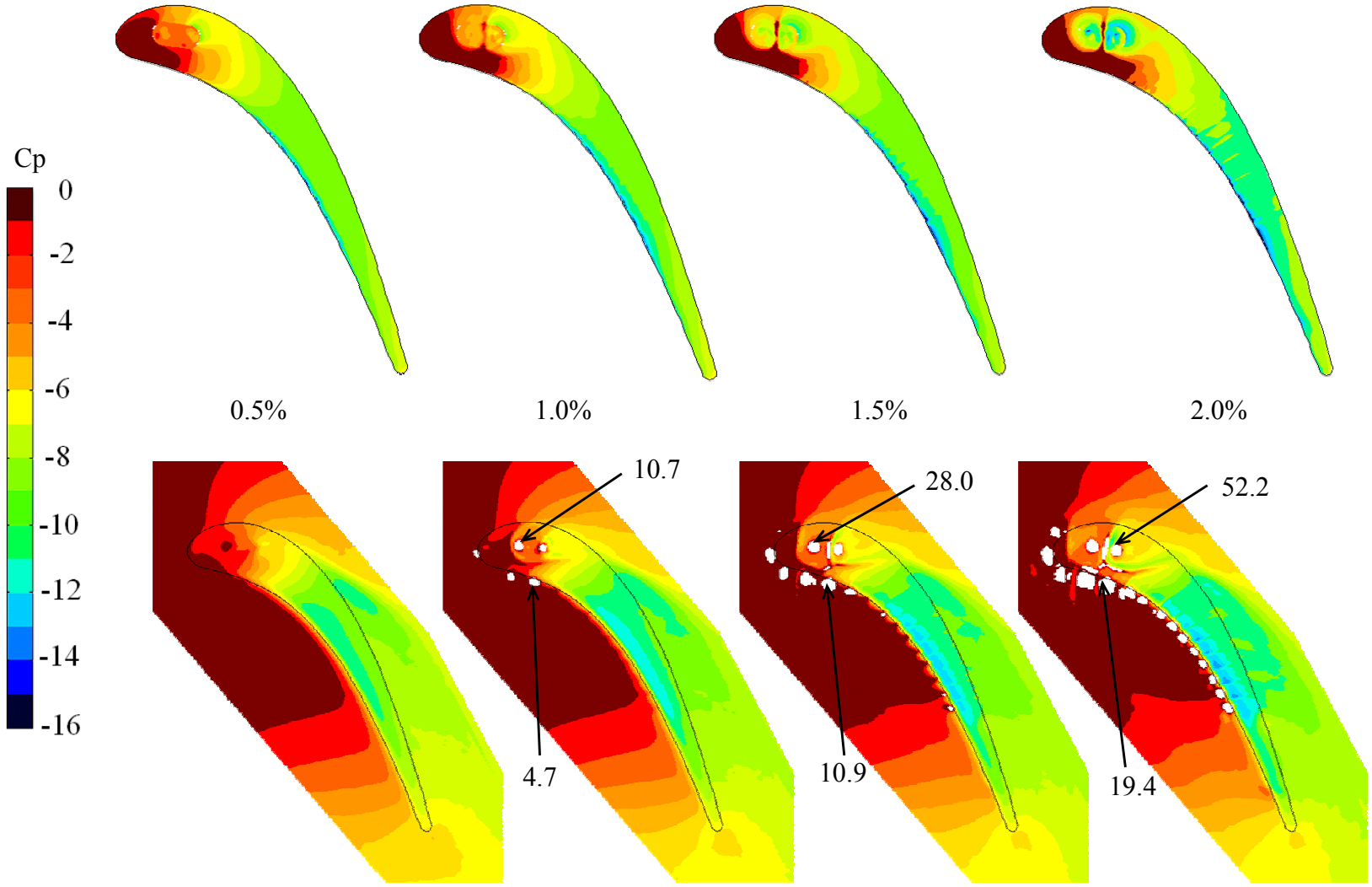

Figure 5.26. Predicted pressure contours along the blade tip and shroud for a microcircuit and dirt purge with a small tip gap and blowing ratios of 0.5%, 1.0%, 1.5%, and 2.0% core flow. High pressure is noted when values exceed the scale.

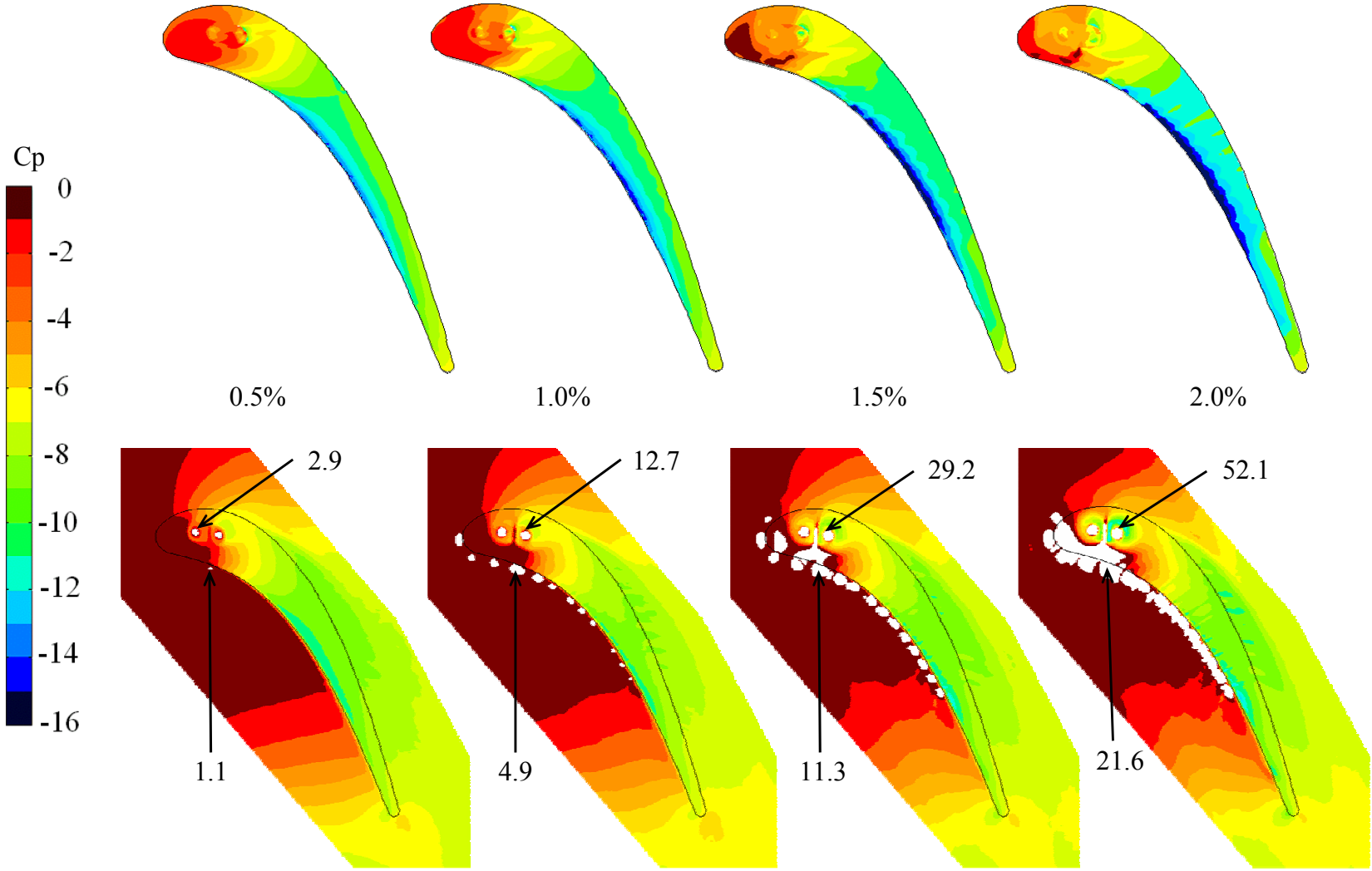

Figure 5.27. Predicted pressure contours along the blade tip and shroud for a microcircuit and dirt purge with a large tip gap and blowing ratios of 0.5%, 1.0%, 1.5%, and 2.0% core flow. High pressure is noted when values exceed the scale.

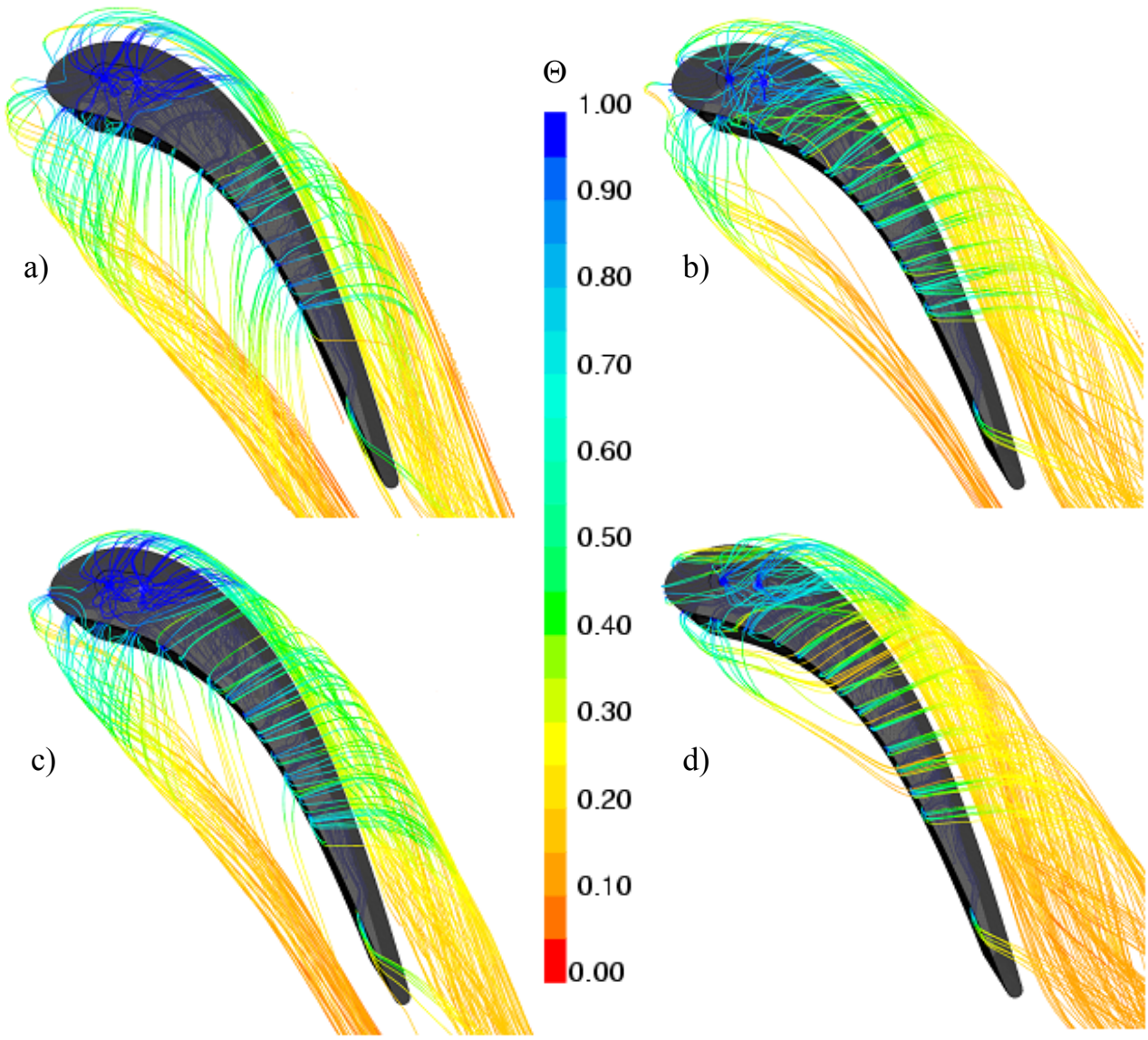

Figure 5.28a-d. Streamlines colored by non-dimensional temperature that are released from the plenum within the blade cavity before exiting the main flow via microcircuit and dirt purge ducts for a a) small tip and 1.5% blowing, b) large tip and 1.5% blowing, c) small tip and 1.0% blowing and d) large tip and 1.0% blowing.

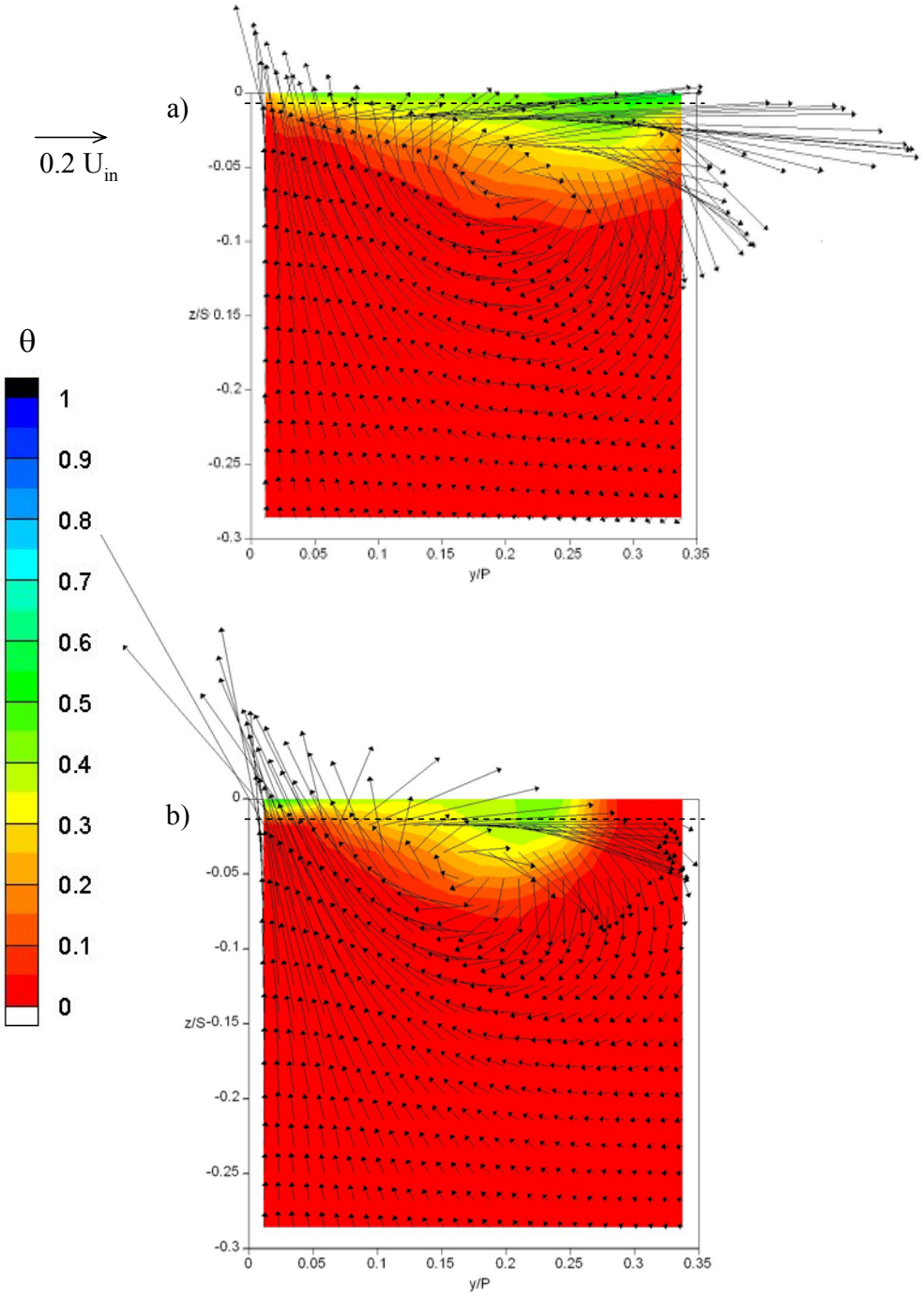

Figure 5.29a-b. Secondary flow vectors with contours of temperature plotted along a pressure side plane (PS2) defined as being normal to the blade at an axial chord location of 30% for microcircuit cooling with a a) small tip gap and 1.5%, and b) large tip gap and 1.5% blowing.

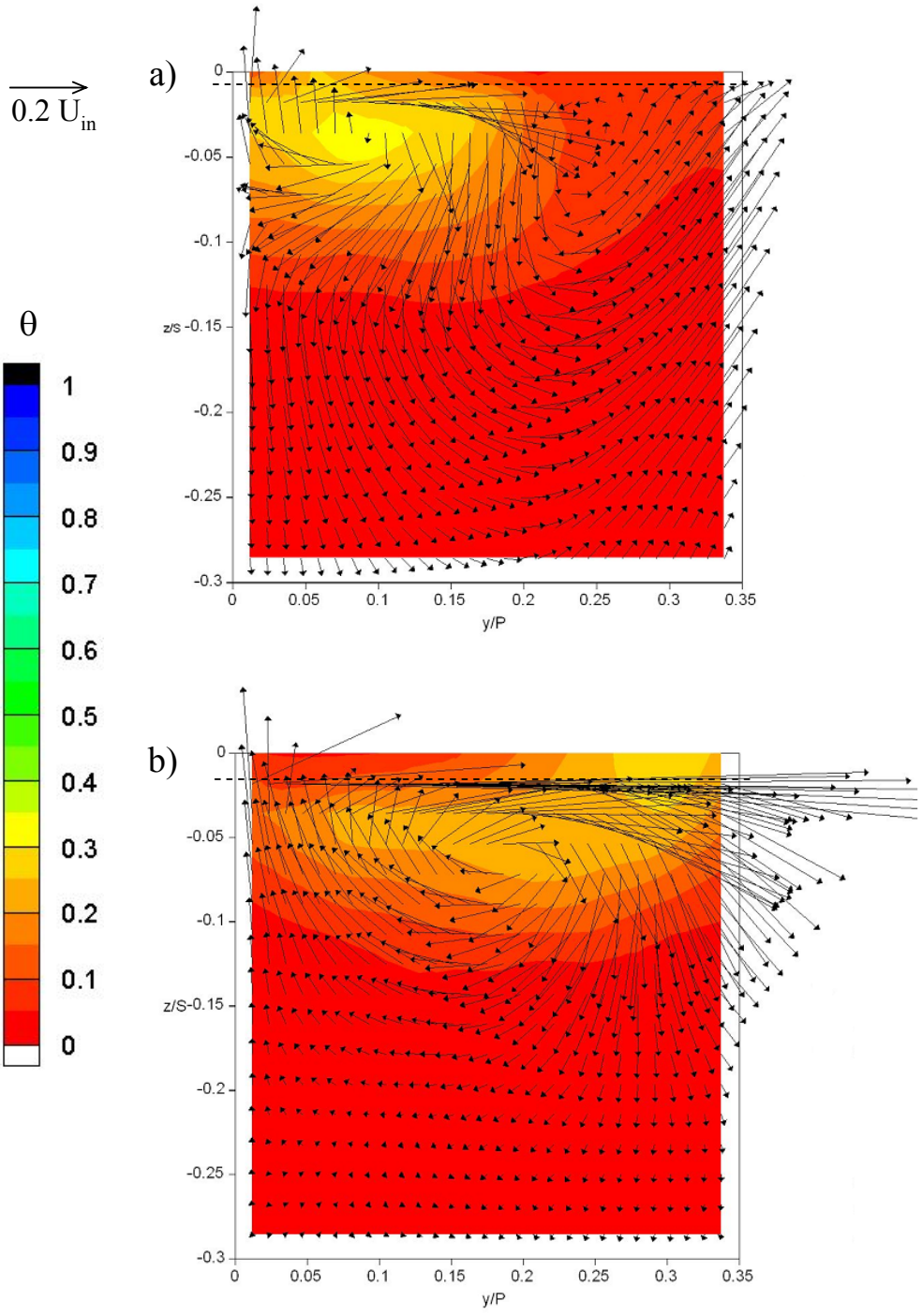

Figure 5.30a-b. Secondary flow vectors with contours of temperature plotted along a suction side plane (SS6) defined as being normal to the blade at an axial chord location of 94% for microcircuit cooling with a a) small tip gap and 1.5%, and b) large tip gap and 1.5% blowing.

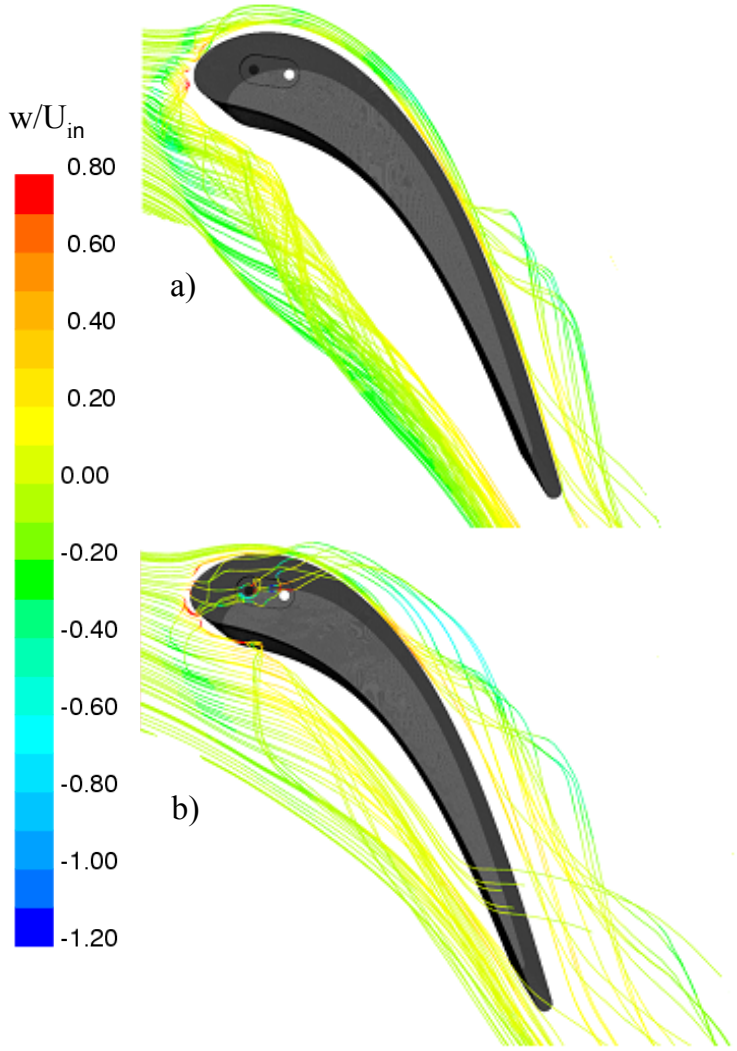

Figure 5.31a-b. Streamlines released from 1.5 tip gap heights below the shroud that are colored by the non-dimensional spanwise velocity component for microcircuit and dirt purge coolant with a a) small tip and 1.5% blowing, and b) large tip and 1.5% blowing.

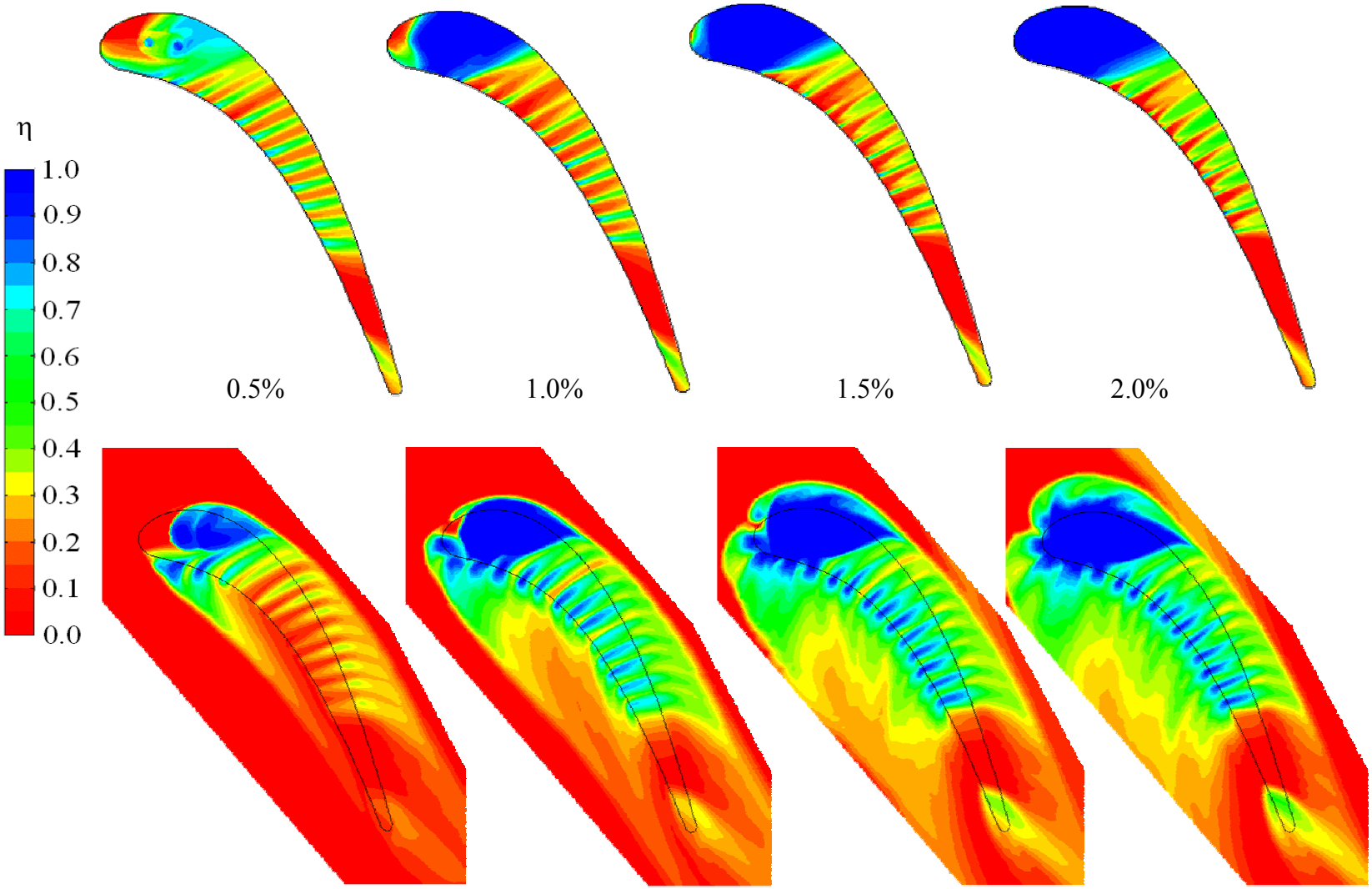

Figure 5.32. Predicted adiabatic effectiveness contours along the blade tip and shroud for a microcircuit and dirt purge with a small tip gap and blowing ratios of 0.5%, 1.0%, 1.5% and 2.0% core flow.

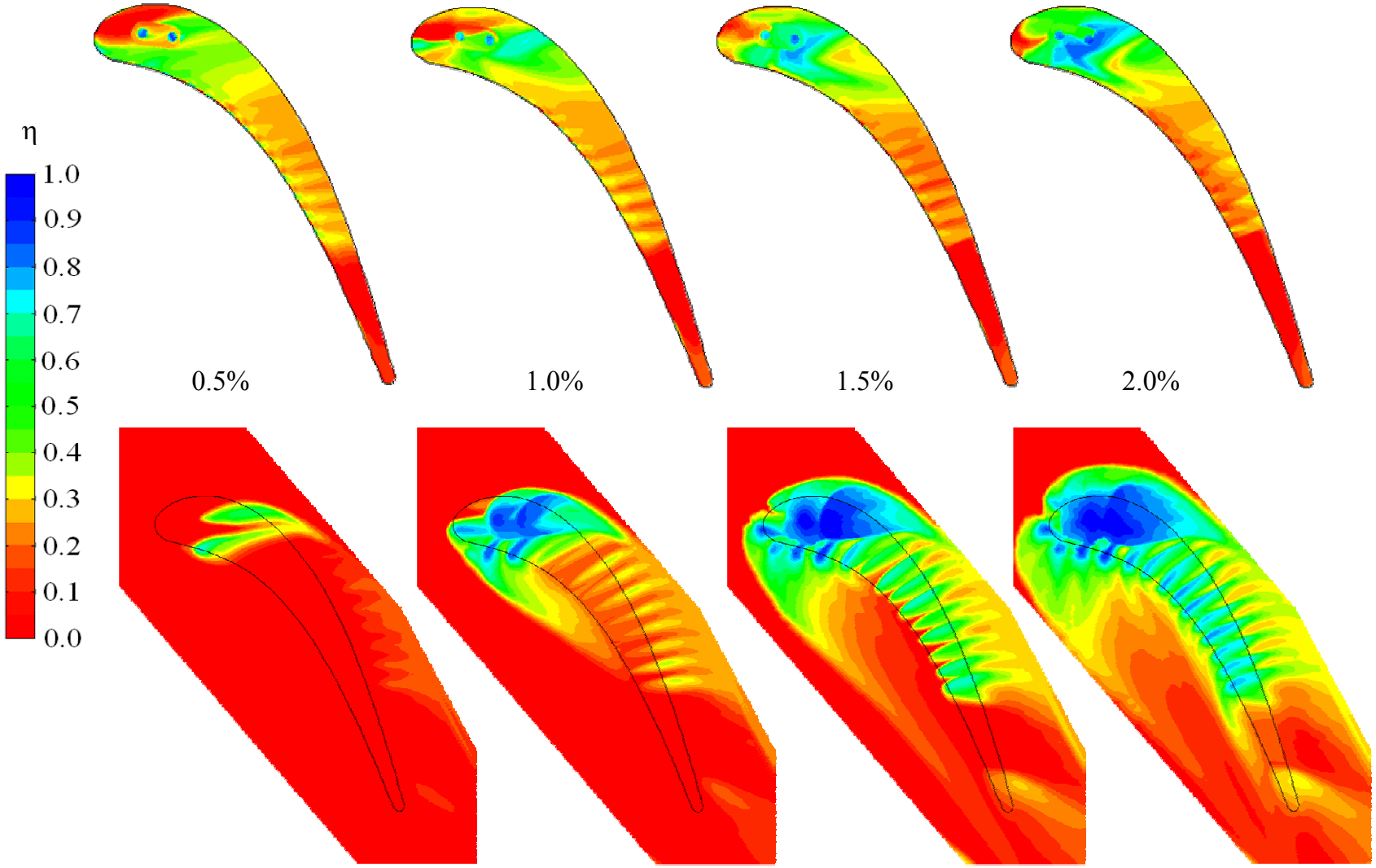

Figure 5.33. Predicted adiabatic effectiveness contours along the blade tip and shroud for a microcircuit and dirt purge with large tip gap and blowing ratios of 0.5%, 1.0%, 1.5% and 2.0% core flow.

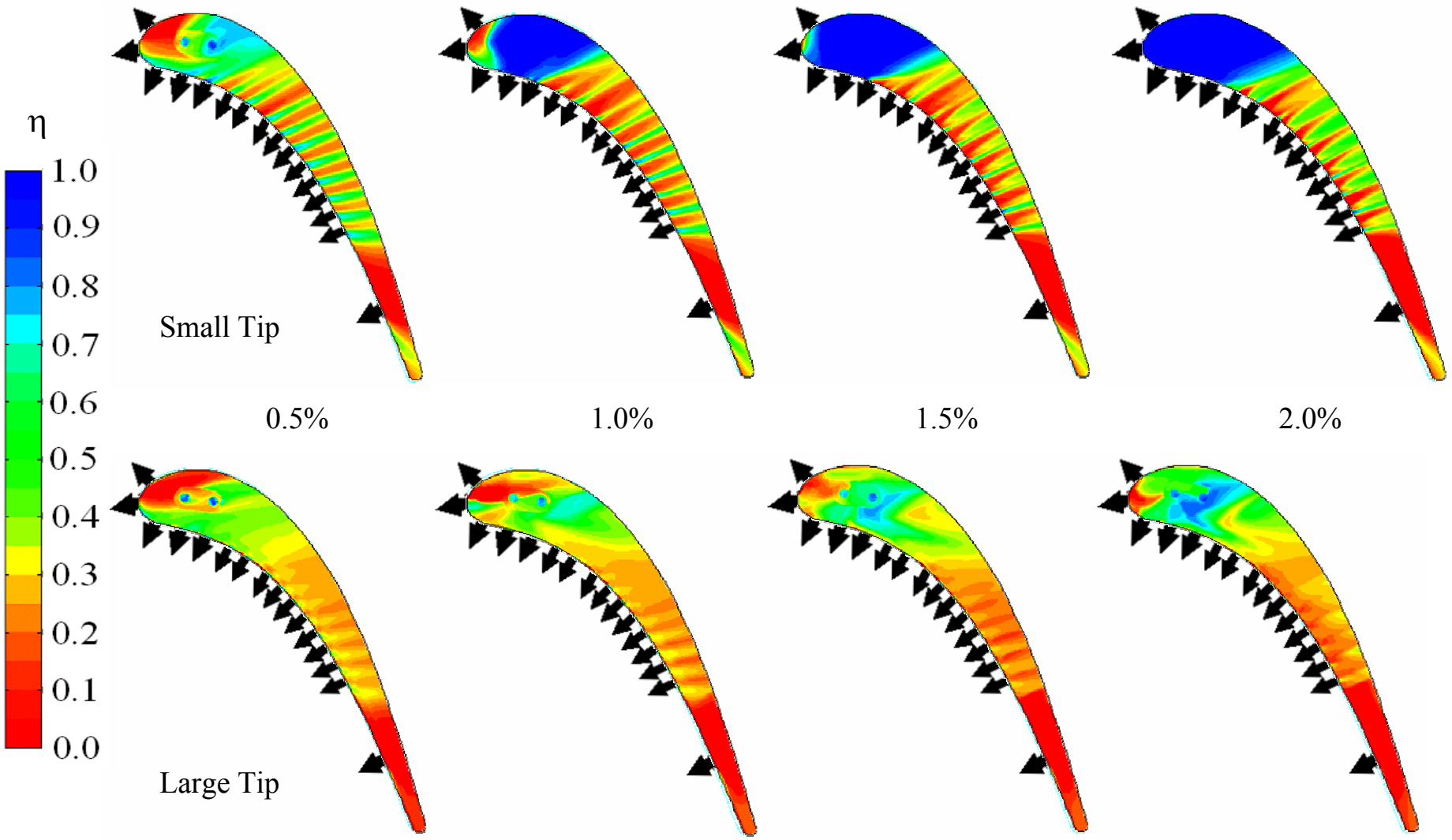

Figure 5.34. Predicted adiabatic effectiveness contours along the blade tip for small and large tip gaps with microcircuit blowing ratios of 0.5%, 1.0%, 1.5% and 2.0% core flow. The arrows around the blade indicate the microcircuit exits.

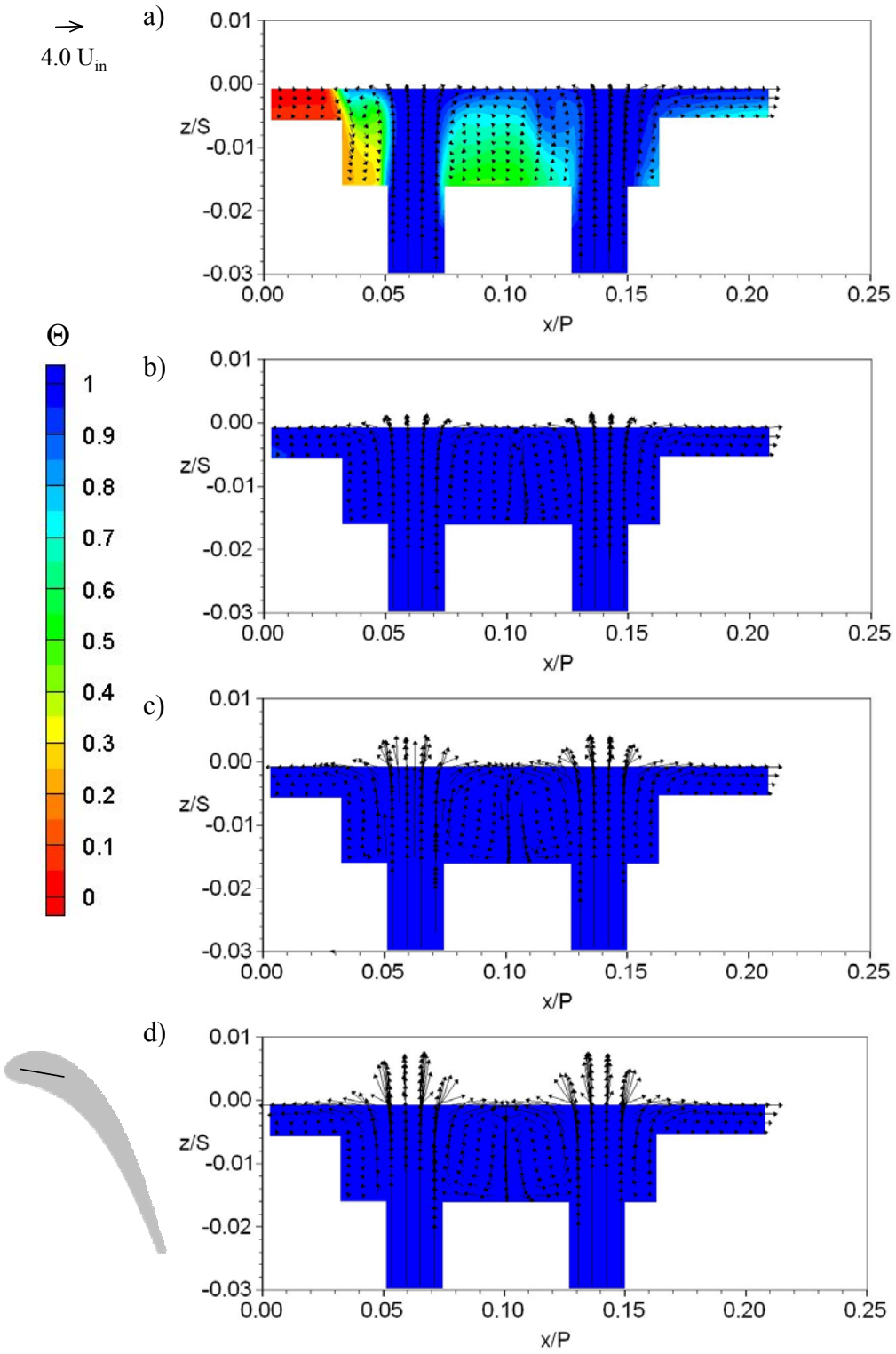

Figure 5.35a-d. Cross-sectional view of the dirt purge cavity for microcircuit and dirt purge cooling with a small tip gap and a) 0.5%, b) 1.0%, c) 1.5%, and d) 2.0% blowing.

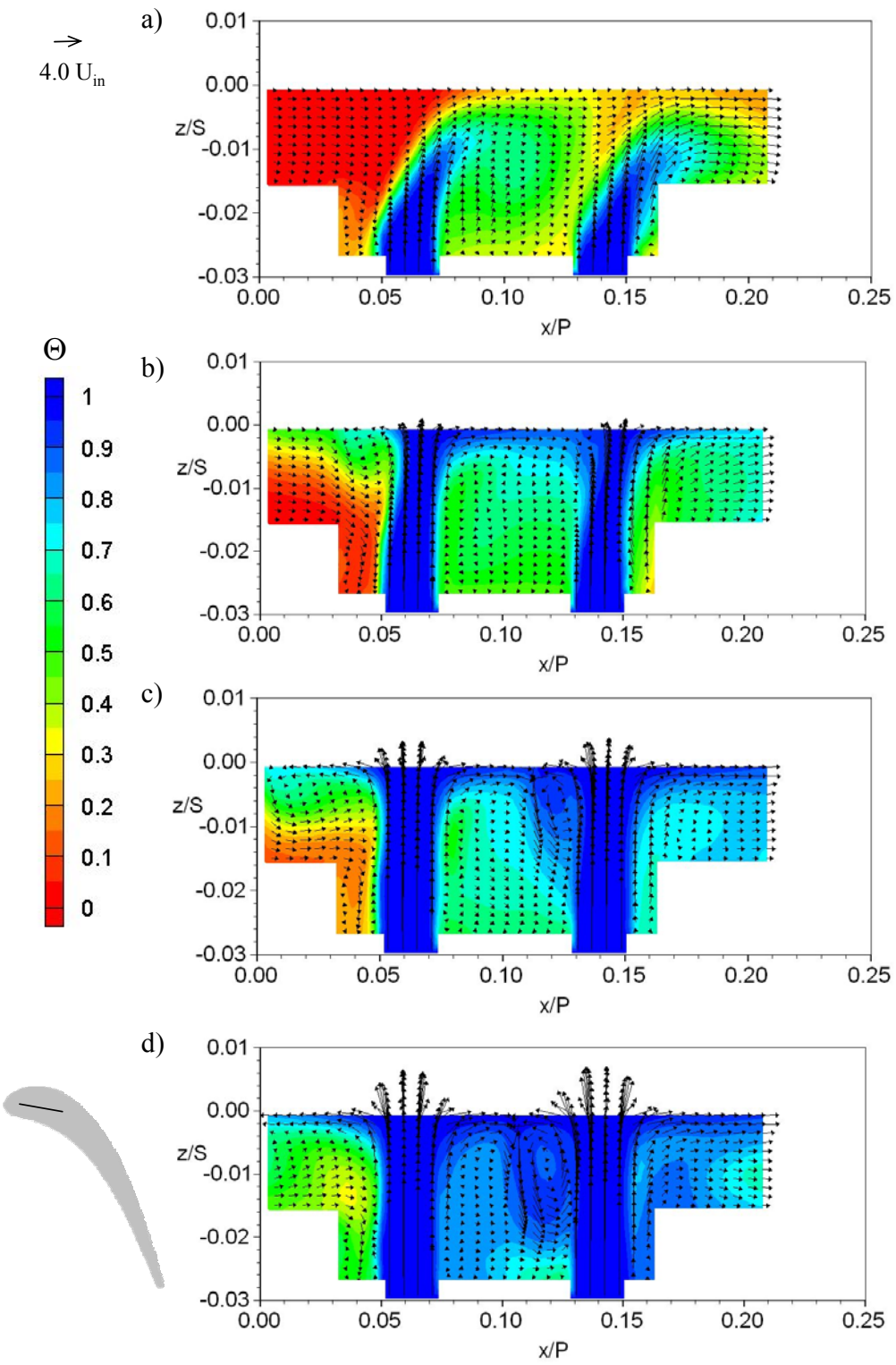

Figure 5.36a-d. Cross-sectional view of the dirt purge cavity for microcircuit and dirt purge cooling with a large tip gap and a) 0.5%, b) 1.0%, c) 1.5%, and d) 2.0% blowing.

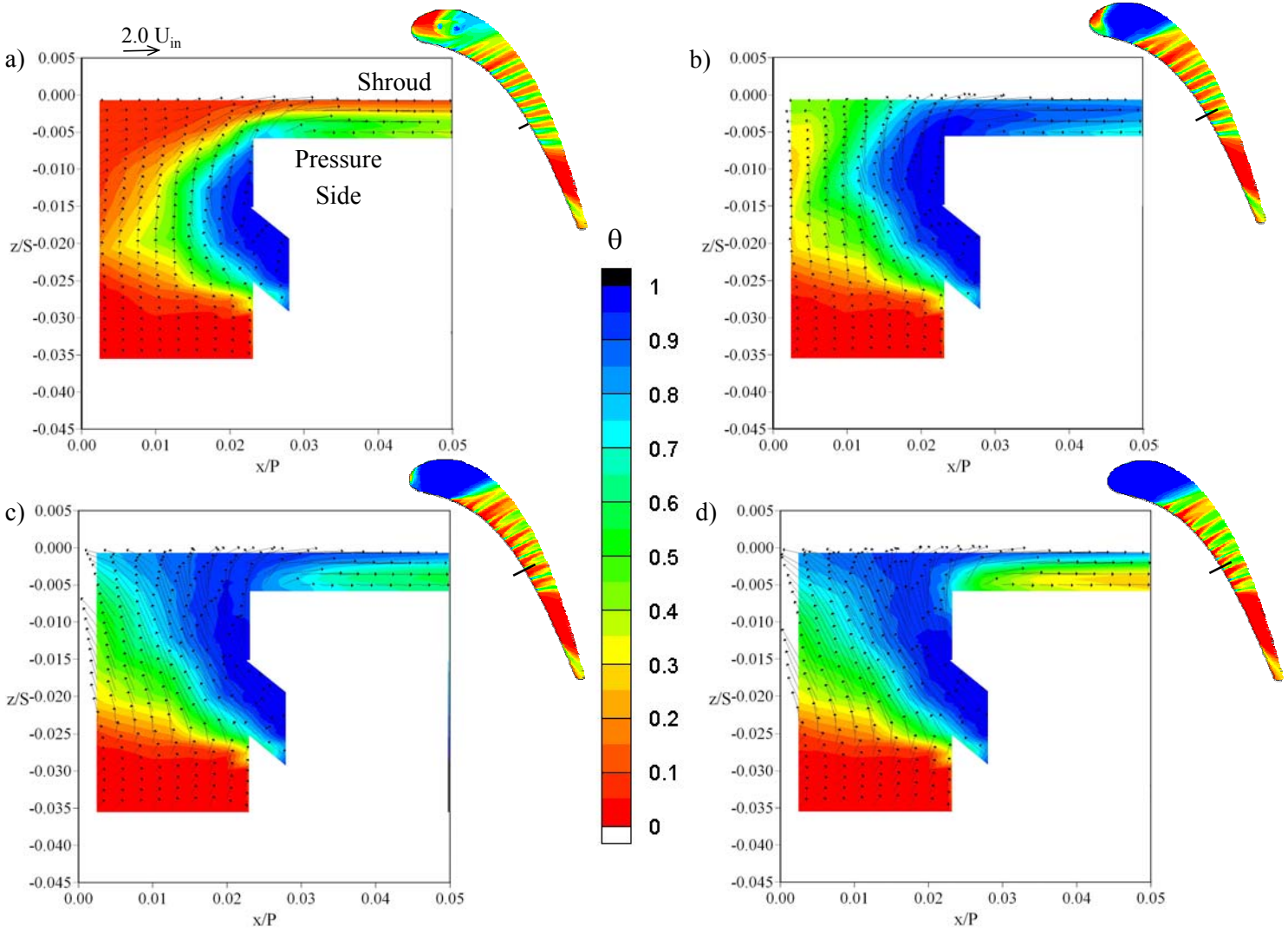

Figure 5.37a-d. Mid-chord blade cross-section through a microcircuit duct showing the coolant path for associated with a small tip gap and a) 0.5%, b) 1.0%, c) 1.5%, and d) 2.0% blowing.

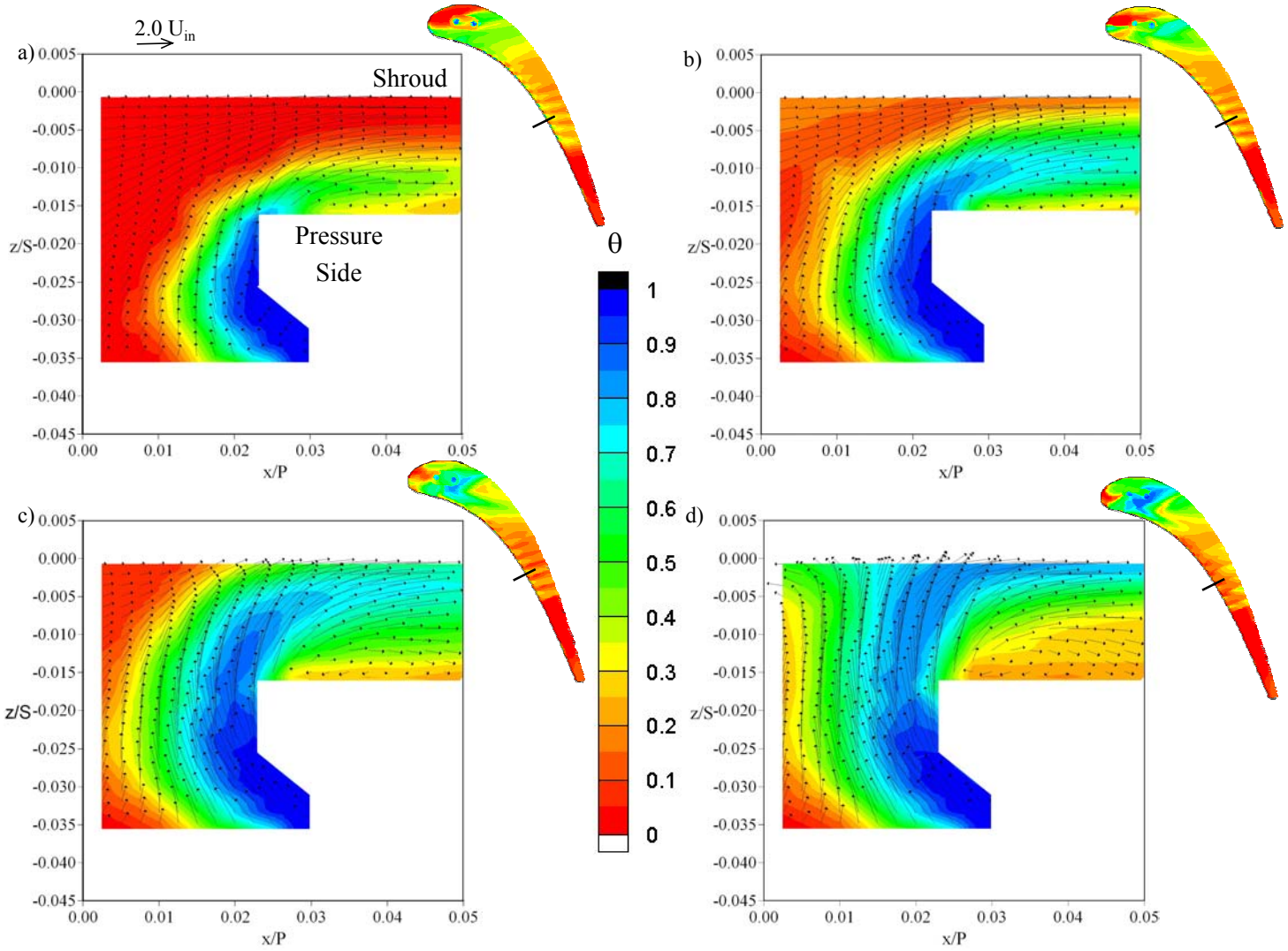

Figure 5.38a-d. Mid-chord blade cross-section through a microcircuit duct showing the coolant path for a large tip gap and a) 0.5%, b) 1.0%, c) 1.5%,and d) 2.0% blowing.

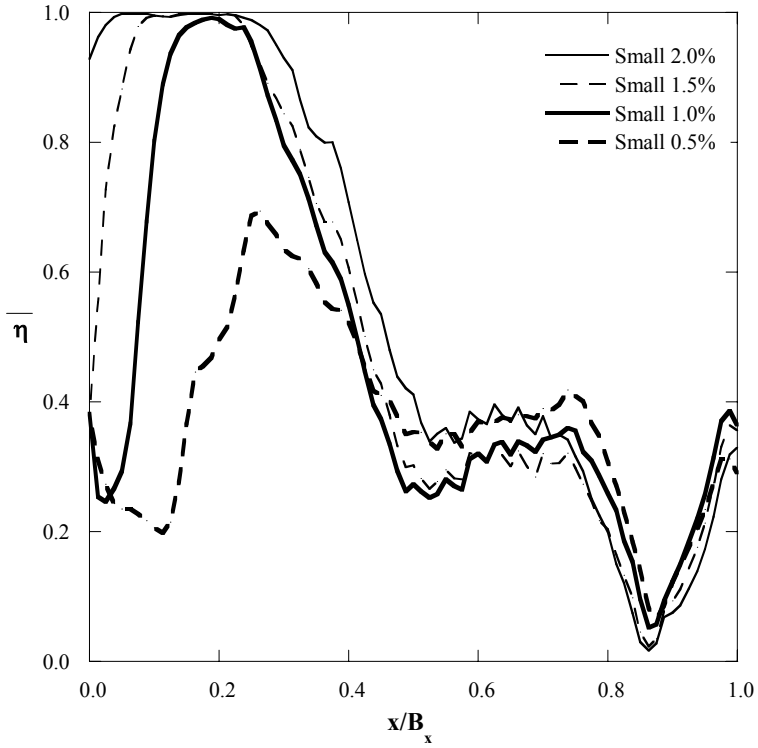

Figure 5.39. Comparison of pitchwise-averaged effectiveness along the tip for the small tip gap with microcircuit and dirt purge blowing.

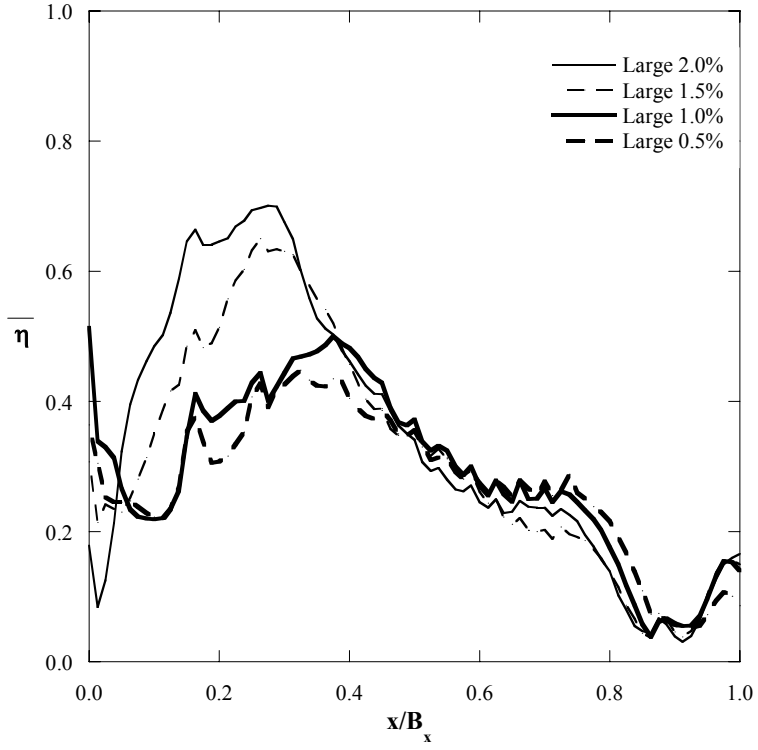

Figure 5.40. Comparison of pitchwise-averaged effectiveness along the tip for the large tip gap with microcircuit and dirt purge blowing.

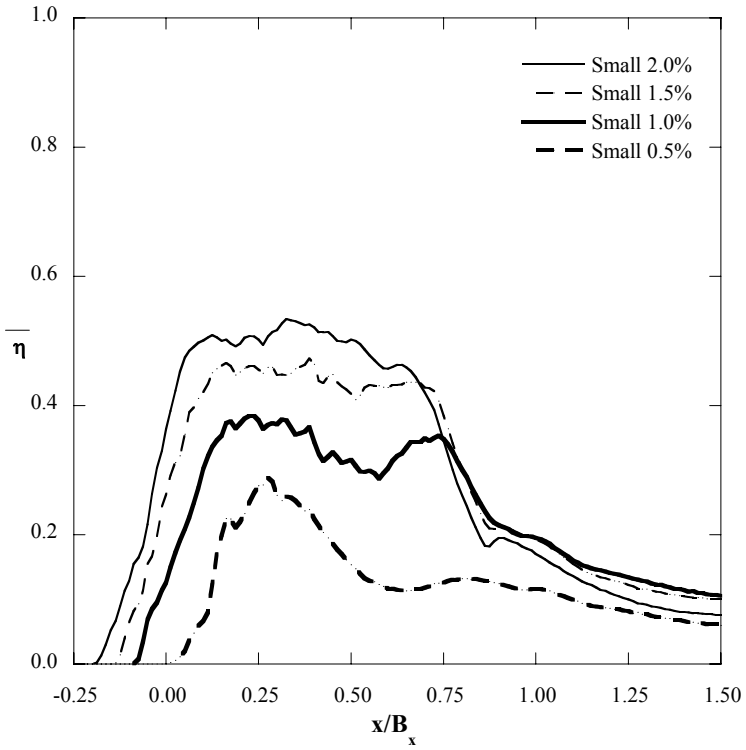

Figure 5.41. Comparison of pitchwise-averaged effectiveness along the shroud for the small tip gap with microcircuit and dirt purge blowing.

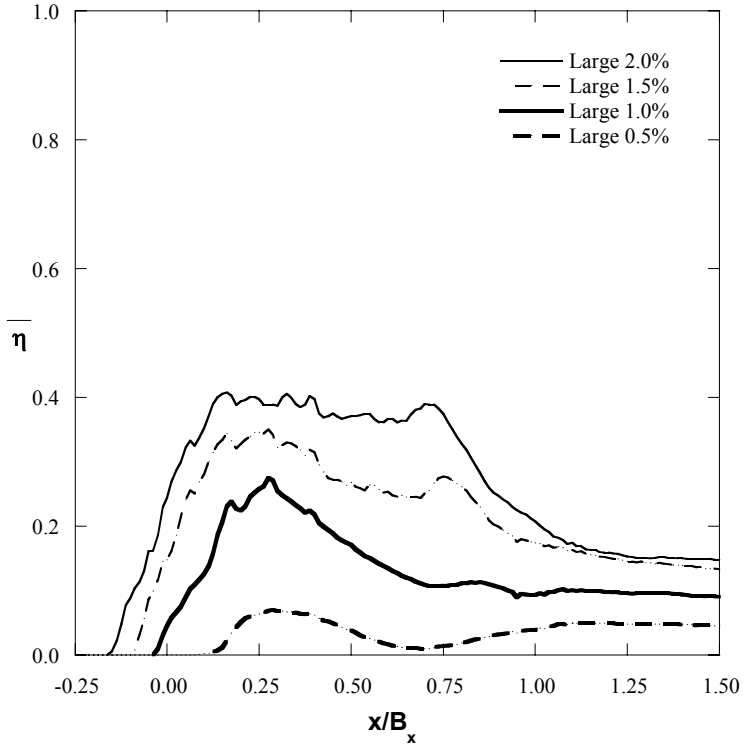

Figure 5.42. Comparison of pitchwise-averaged effectiveness along the shroud for the large tip gap with microcircuit and dirt purge blowing.

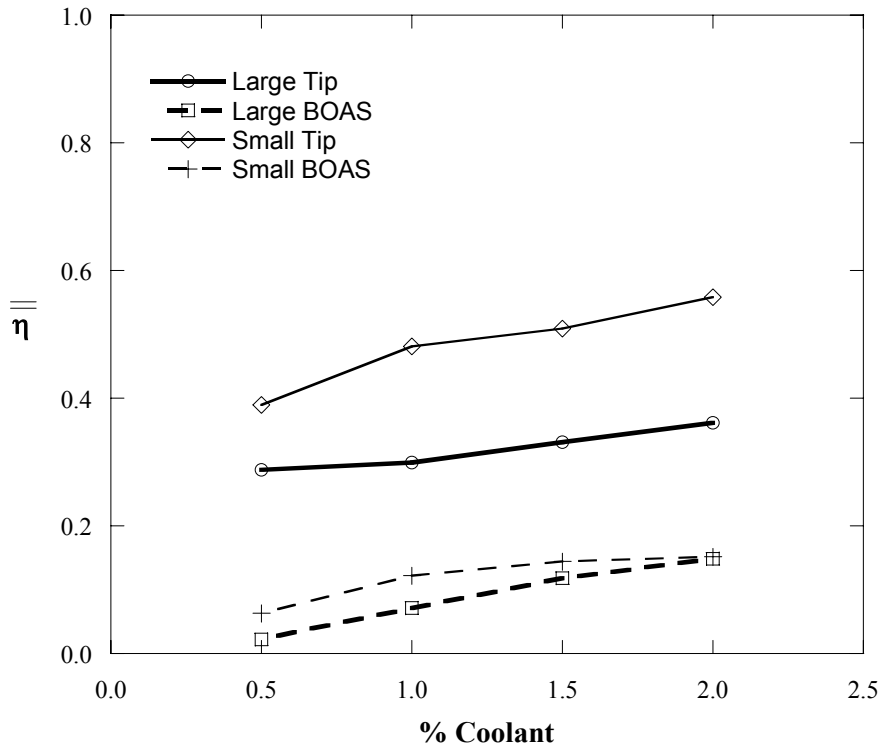

Figure 5.43. Area-averaged effectiveness along the tip and shroud plotted against coolant mass flow rates.